Microchimica Acta (2020) 187: 612
https://doi.org/10.1007/s00604-020-04460-y

REVIEW ARTICLE

Gold nanotubes: synthesis, properties and biomedical applications

Yan-ling Liu[1] · Jian Zhu[1] · Guo-jun Weng[1] · Jian-jun Li[1] · Jun-wu Zhao[1]

Received: 4 March 2020 / Accepted: 16 July 2020 / Published online: 16 October 2020

Abstract

This review (with 106 references) summarizes the latest progress in the synthesis, properties and biomedical applications of gold nanotubes (AuNTs). Following an introduction into the field, a first large section covers two popular AuNTs synthesis methods. The hard template method introduces anodic alumina oxide template (AAO) and track-etched membranes (TeMs), while the sacrificial template method based on galvanic replacement introduces bimetallic, trimetallic AuNTs and AuNT-semiconductor hybrid materials. Then, the factors affecting the morphology of AuNTs are discussed. The next section covers their unique surface plasmon resonance (SPR), surface-enhanced Raman scattering (SERS) and their catalytic properties. This is followed by overviews on the applications of AuNTs in biosensors, protein transportation, photothermal therapy and imaging. Several tables are presented that give an overview on the wealth of synthetic methods, morphology factors and biological application. A concluding section summarizes the current status, addresses current challenges and gives an outlook on potential applications of AuNTs in biochemical detection and drug delivery.

Keywords Gold nanotubes · Synthesis · Protein transportation · Biosensor · Photothermal therapy

Introduction

Since the discovery of carbon nanotubes in 1991 [1], noble metal tubular nanostructures have aroused great interest because of combination of properties from the metal components and good biocompatibility, especially gold nanomaterials. In the last decades, different types of gold nanoparticles (AuNPs) have been reported in the literature due to their countless biomedical applications [2], including biosensors [3], targeted drug delivery [4], catalysis [5], drug release, photothermal therapy [6] and molecular imaging [7]. These applications are based on features such as possibility of tuning of particle size (for desired electrical, optical properties), biocompatibility, stability and large surface areas [8]. However, gold nanotubes have several unique advantages compared with other gold nanomaterials, such as being easy to functionalize with various ligands and drugs, higher surface-to-volume ratios than their solid counterparts, superior load-carrying ability and malleable to various sizes and shapes [9].

The synthesis of AuNTs has attracted much enthusiasm because of their unique electronic and optical properties. Perhaps the most conceptually simple method to generate gold nanotubes is to confine their growth with templates. The nanoscale channels in track-etched membranes (polycarbonate) and Anodic Alumina oxide template (AAO) have been widely used for this reason [10]. But in many cases, the templates have to be removed in the post-synthesis step so that the nanostructure can be put into use [11]. In general, hard template-based methods are not easy to scale up to produce nanostructures for commercial applications quickly and cheaply. This realization lead Xia and his team to develop template-engaged replacement reaction: a one-step approach to the large-scale synthesis of metal nanostructures with hollow interiors, including gold nanotubes [12]. Their porosity and wall thickness can be controlled by changing experimental conditions [13]. Furthermore, the plasmon resonance frequency of gold nanotubes can be tuned in the range of visible to near infrared by controlling their dimensions and morphology. For example, the absorption peak of AuNTs blue-shifts with increasing thickness of wall [14] and red-shifts with increasing nanotube length [15].

Unique intrinsic features of gold nanotube are fundamental to major biomedical applications. Up to now, AuNTs have

✉ Jian Zhu
zhujian@xjtu.edu.cn

✉ Jun-wu Zhao
nanoptzhao@163.com

[1] The Key Laboratory of Biomedical Information Engineering of Ministry of Education, School of Life Science and Technology, Xi'an Jiaotong University, Xi'an 710049, People's Republic of China

been widely applied in catalysis [16], chemical separations and analysis [17], biosensing [18, 19], photothermal therapy [15], photoacoustic imaging [20], protein transportation [21] and so on. The optical properties of AuNTs present possibilities that can be applied to cell therapies that involve photothermal ablation and light triggered drug delivery [16]. In this paper, we first summarized different synthesis methods and properties of AuNTs. Then, the factors which may influence the morphology and properties of AuNTs were also discussed. Finally, we reviewed the biomedical application progress of gold nanotubes in biosensor, protein transport, photothermal therapy and medical imaging.

Synthesis

The template method of synthesizing AuNTs, as an alternative to conventional lithography methods, is one of the most versatile, rapid, facile and economic approaches toward hollow structures. In a typical process, this method is divided into two steps: template design and synthesis, and "patterning" of desired materials, possibly followed by template removal [22]. Recently, the template synthesis mechanism has been well understood, such as electrodeposition via voltage control, galvanic replacement and controllable chemical transformation, enabling a wide range of hollow nanotubes. The synthetic strategies of gold nanotubes can be divided into hard templates and sacrificial templates according to their different structures.

Hard template method

The hard template method is well known for its usefulness and reliability in controlling the size and shape of hollow structures. Gold nanotubes are obtained by coating the target material on a rigid core with a desired shape to form a shell, and then removing the core. For example, Dong et al. reported a method for the fabrication of ordered hollow gold nanotubes by using a combination of double templates (NCP silica template and PS template) and electroless plating [23]. Template is the prerequisite for preparing nanotubes. The most common preparation methods of AuNTs by hard template are electrochemical deposition and chemical deposition. The universal hard template materials synthesized AuNTs are divided into Anodized Alumina oxide template and track-etched membranes (TeMs) depending on the types of template.

Anodic alumina oxide template

Anodic Alumina oxide template (AAO) with uniform and parallel pores is made by anodic oxidation of aluminium sheet in solutions of sulphuric, oxalic or phosphoric acids. According to the oxidation potential added during electrolysis, Aluminium oxide films with different pore sizes can be obtained with different electrolyte types and electrolysis time. The maximum pore diameter is hundreds of nanometres, the minimum is 5 nm and the density of pore is as high as 10^{11} pores/cm^2, pore sizes ranging from 10 nm to 100 μm can be made [24–26]. The porous alumina template has a single hole diameter, high temperature resistance and high strength, which is the most widely used template so far [10, 27–29].

The typical method for fabrication of gold nanotube arrays is summarized in Fig. 1 by AAO template [30–32]. Firstly, a nanoporous AAO template (Fig. 1a) is fabricated on substrate by anodizing an aluminium thin film on a thin gold underlayer. Polypyrrole is deposited into the AAO pores (Fig. 1b) by electropolymerization. The AAO pores are then chemically etched using NaOH, creating shells around the polypyrrole nanorods (Fig. 1c). Gold is then electrodeposited into the shells (Fig. 1d). At the next stage, the polypyrrole is removed by plasmon etching (Fig. 1e). An outer shell is then formed by chemical etching as before. If the etch is continued, the AAO matrix is completely removed to reveal freestanding arrays of gold nanotubes attached to the substrate (Fig. 1f). The morphology and composition of AuNTs can be tuned by controlling the deposition parameters. For instance, the change of the wire to tubular structure is by adjusting pH of gold plating bath. The higher alkalinity is prone to form the tubular structure owing to the numbers of nuclei are fewer under this condition, while the lower alkalinity is favourable to the formation of wire structure [33]. The inner diameter of gold nanotubes becomes smaller upon the increase in deposition time of plating bath [34–36].

In another study, Bridges synthesized solution suspendable gold nanotubes on template-directed electrochemical synthesis (TES) in porous AAO using different sacrificial polymer core preparations (Fig. 1h). The method based on the hydrophobic collapse of a sacrificial poly(3-hexyl) thiophene core that did not use etching steps [28, 38]. The result revealed that the wall thickness of the gold nanotubes could be varied by varying polymer core hydrophobicity (Fig. 2).

Track-etched membranes

Track-etched membranes (TeMs) are obtained by bombarding a nanoporous polycarbonate sheet with nuclear fission fragments to generate damage tracks, and then chemically etching these tracks into pores [39]. TeMs can serve as matrices for the preparation of ordered arrays of metallic micro and nanostructures with unique physical properties [40–44]. The TeMs commonly used in the preparation of gold nanotubes are mainly polycarbonate template (PC) [45] and polyethylene terephthalate (PET) [16, 46]. The method of fabricating AuNTs on nanoporous polycarbonate template by electrodeposition method illustrated in Fig. 1g [37]. In general, the

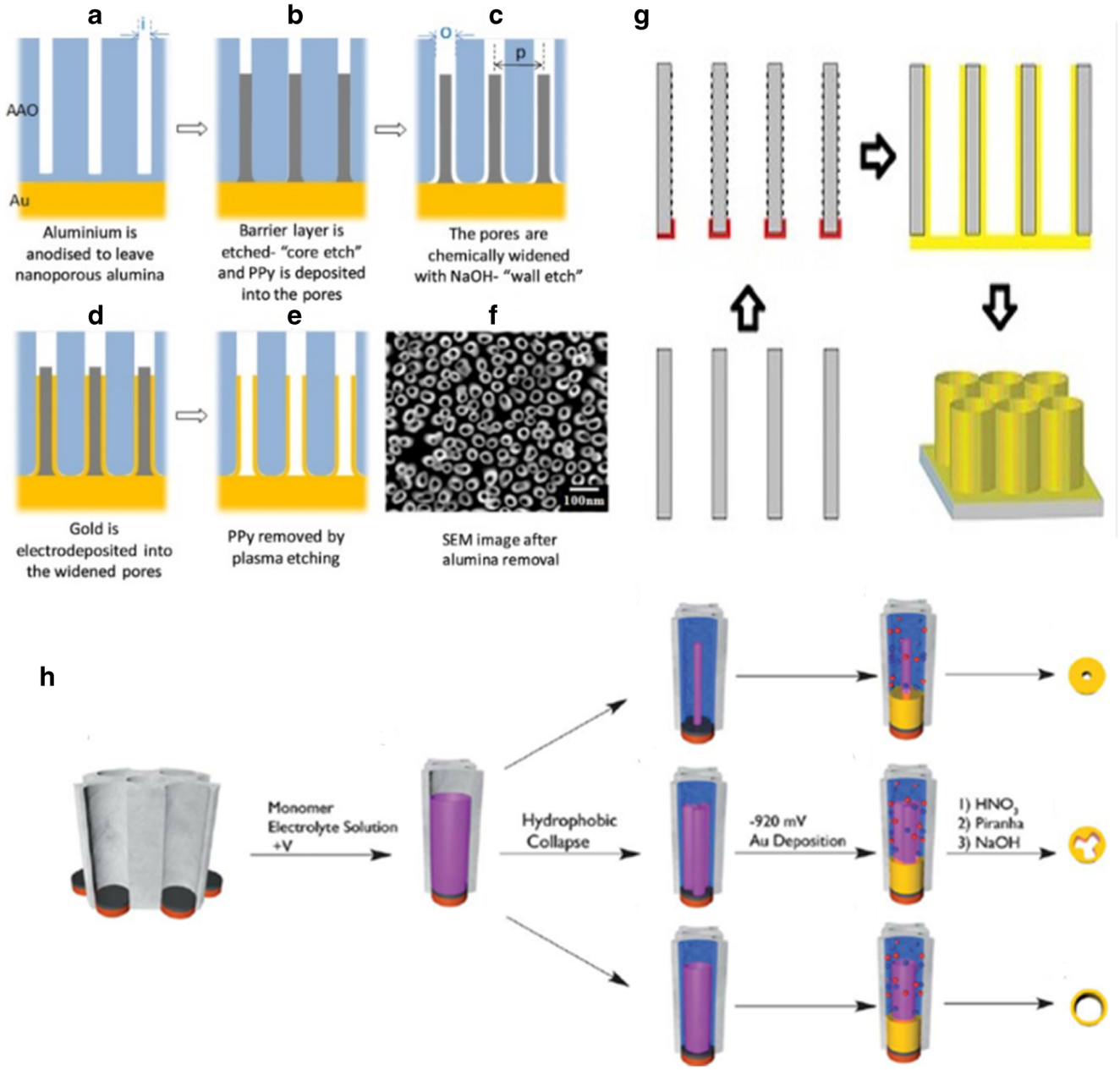

Fig. 1 **a**–**e** Summary of the fabrication process for gold nanotube arrays, where i is the inner diameter, o is the outer diameter and p is the pitch. **f** Plane view SEM image of the final structure. Reprinted with permission from ref. [31]. Copyright 2011 IOP science. **g** The schematic illustration of the AuNTs synthesis on nanoporous polycarbonate template. Reprinted with permission from ref. [37]. Copyright 2019 Elsevier B.V. **h** Scheme and proposed mechanism of gold nanotube synthesis. Reprinted with permission from ref. [38]. Copyright 2013 Royal Society of Chemistry

length of gold nanotubes was determined by the membrane thickness, but Pyo and co-workers prepared gold nanotube of various lengths and pore sizes controlled by adjusting plating temperatures and solution compositions [47]. They found that the length of nanotubes and the thickness of gold film decrease with the increase in plating temperature. Long nanotubes can be obtained by depositing Au at the interface at relatively low temperature (4 °C) and these nanotubes run through the whole film thickness with small openings. In addition, AuNTs were synthesized by the electroless template approach in the pores of ion track membranes based on polyethylene terephthalate(PET). The wall thickness of Au and Ag/Au NTs was determined to be 35.8 ± 9.0 and 77.8 ± 6.1 nm respectively [41]. Moreover, the morphology and metal components of AuNTs can be also changed. For instance, Mollamahale et al. introduced a novel and highly sensitive nanoelectrode through electrodeposition of gold nanotubes inside polycarbonate (PC) membrane and then developing

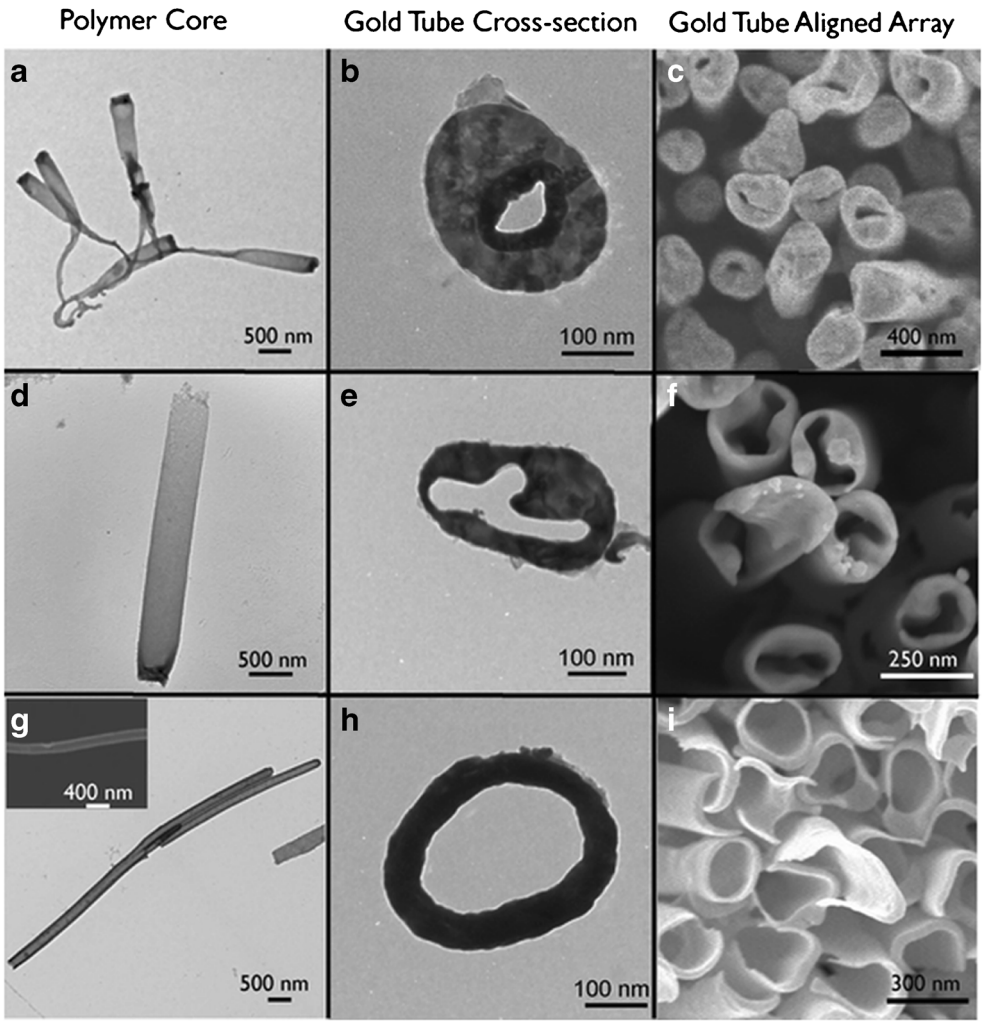

Fig. 2 TEM images of the polymer core (first column), resulting gold ring (second column) and SEM images of the corresponding nanotube array (third column). Within each row are a series of corresponding images (core, ring, tube). Reprinted with permission from ref. [38]. Copyright 2013 Royal Society of Chemistry

three-dimensional gold nanoelectrode ensembles [45]. Tao's group reported Pt-Au alloy nanotube array which was produced by electrodepositing strategy using nanopore polycarbonate (PC) membrane at −0.35 V [48]. Siwy and co-workers described a single conically shaped gold nanotube embedded within 12-μm-thick polyethylene terephthalate (PET) [49].

AAO templates and TeMs are most commonly used for the synthesis of AuNT arrays. Both templates are very convenient to use during the growth of AuNTs by various growth mechanisms, but each type of template also has a few disadvantages. Take PC membrane for example, the advantage of using PC as template is that it is easy to be pyrolyzed and removed at high temperature, but the flexibility of PC is easier to distort during the heating process, and the template is removed before the nanotubes are completely densified. These factors can lead to breakage and deformation of nanotubes. However, the advantage of using AAO as template is its rigidity and high-temperature resistance, which makes the nanorods densified completely before removal. This would result in a much larger surface area of relatively freestanding and unidirectionally aligned nanotube arrays. The disadvantage with AAO is to completely remove the template after the growth of nanotube.

Sacrificial templates method based on galvanic replacement

Compared with the hard template method, the sacrificial templates method is preferred in practical applications. Usually, the templates can be completely oxidized in solution during the formation of the hollow structure. Therefore, the complicated removal steps can be avoided, lowering the production cost and heightening the possibility of scaling-up [22]. Galvanic replacement is a redox process, which can be broken down into two half reactions: the oxidation (loss of electrons) and corrosion of the first metal at the anode and the reduction (gain of electrons) of the ions of the second metal, and subsequent deposition, of this metal at the cathode. The driving force for this reaction comes from the difference in reduction potentials of the two metals involved, with the potential of the second metal necessarily being higher than that of the first

metal. To date, based on the mechanism of galvanic replacement, there are many precursor templates for the synthesis of gold nanotubes, including silver nanowires [9], silver nanorods [15], core–shell Au@Ag nanorods [50], copper nanowires [51], MgO Nanowires [52], sodium sulfate (Na_2SO_4) nanowires [53], SiO_X nanowires [54], cobalt Nanoparticles [55], Au@Ag bimetallic nanowires [56], CdSe nanotube array templating [57] etc.

Bimetallic AuNTs

Nowadays, silver nanowires have been the hottest point in the field of gold nanotubes in the various routes. Because of the perfect crystallographic match, and no additional procedures are required to remove the template after the reaction is completed. Different synthetic approaches could lead to the discovery of different silver nanowires with new properties. For example, there are high purity cylindrical silver nanowires selectively prepared by kinetic control of hydrothermal conditions [58], Ag nanowire arrays grown on nanograted silicon structures [59], pentagonal Ag nanowires prepared by the polyol process and so on. For the synthesis of silver nanowires, a large number of routes have been developed in recent years. However, pentagonal silver nanowires synthesized from soft solutions have become the most popular. Because it is the most feasible way to realize large-scale production of silver nanowires. Xia et al. first proposed the synthesis of gold nanotubes using silver nanowires prepared by PVP (polyvinylpyrrolidone)-assisted polyol method as templates [12]. The standard reduction potential of Ag^+/Ag pair (0.80 V, vs SHE) is lower than that of $AuCl_4^-/Au$ pair (0.99 V, vs SHE). After the $AuCl_4^-$ ions are added into solution of Ag nanowires, Ag nanowires are oxidized at the anode (Fig. 3g (a). The electrons released from the oxidation reduce $AuCl_4^-$ ions into Au atoms (cathode reaction). The deposition leads to the formation of an essentially complete, thin layer of Au with only several holes at the initial reaction sites (Fig. 3g (b)); The Au coating prevents the underneath Ag from directly contacting and reacting with $AuCl_4^-$ ions. As a result, the etching of Ag nanowire continues at the newly formed surfaces as shown in the illustration of cross section and the resulting Ag^+ ions continue to diffuse out of the cavities through the small holes. When the concentration of $AuCl_4^-$ is high enough, the dissolution of Ag transforms each Ag nanowire into a structure characterized by a hollow interior; Fig. 3g(c) begins the dealloying process and the formation of small pinholes in the nanotube wall; Fig. 3g (d) dealloying continues, forming square holes in the wall; Fig. 3g (e), fragmentation of the porous nanotube into Au nanoparticles with irregular shapes triggered by complete dealloying [12]. Figure 3 **a**–**f** represents a typical SAED pattern taken from an individual nanotube synthesis process. Based on the single-walled gold nanotubes, subsequently, a thin layer of Ag was coated on the nanotube through reduction, followed by another round of galvanic replacement with $HAuCl_4$, resulting in the formation of double-walled nanotubes (Fig. 3h). Repeating this cycle once, more yielded the triple-walled Au-Ag nanotubes. Theoretically, these processes can be further repeated to generate nanotubes with multiple walls [50].

In addition to gold-silver bimetallic nanotubes, there are many other materials as precursor templates for the synthesis of gold nanotubes. For example, Au Porous nanotubes were synthesized by chemical synthesis of Ag nanowire precursors. Subsequently, $[PtCl_6]^{2-}$ was added to form Pt-Au porous nanotubes by galvanic substitution reaction with residual Ag (Fig. 4a) [61]. In another study, Luo's research [51] reported one-pot method for the facile synthesis of Cu nanowires in high purity, together with ultrathin diameters well below 20 nm, and as sacrificial templates for the synthesis of Au nanotubes through the galvanic replacement process. Kim and co-workers [52] prepared MgO nanowires coated with a conformal layer of Au via sputtering. By etching away the MgO core of aqueous $(NH_3)_2SO_4$ solution, hollow nanotube-like structures of Au were obtained.

Trimetallic AuNTs

Galvanic replacement can be easily extended to the three-metal system by changing the reaction conditions, which can be used to produce a variety of unique nanotube structures. Furthermore, the use of more than one metal greatly increases the functional diversity of nanostructures, along with more different properties and new applications. Xia et al. [50] synthesized three-walled nanotubes composed of Au/Ag alloy in the inner wall and Pd/Ag alloy in the outer wall, based on the gold-silver bimetallic nanotubes. Sun et al. [62] chose core-shell structure of Au@Ag nanorods as templates and added K_2PtCl_4 solution to prepare PtAgAu nanotubes by galvanic displacement replacement. The bimetallic nanorod template experienced the structural evolution from nanorod to tip hollow nanorod and finally to porous nanotube. What is interesting is that Au is involved in the displacement reaction in this process (Fig. 4c). The result indicated the selection of self-sacrificed templates for galvanic replacement is not limited to single metal templates. The gold nanotubes synthesized by polymetallic components have broad and potential application prospects.

AuNT-semiconductor hybrid materials

Depositing semiconductor nanostructures on the surface of gold nanotubes not only can improve the stability and durability of metal nanostructures but also improve light absorption and faster transfer of photo-induced charge carriers. For example, Guan et al. [63] synthesized AuAg@CdS double-walled nanotubes (DWNTs) through a three-steps

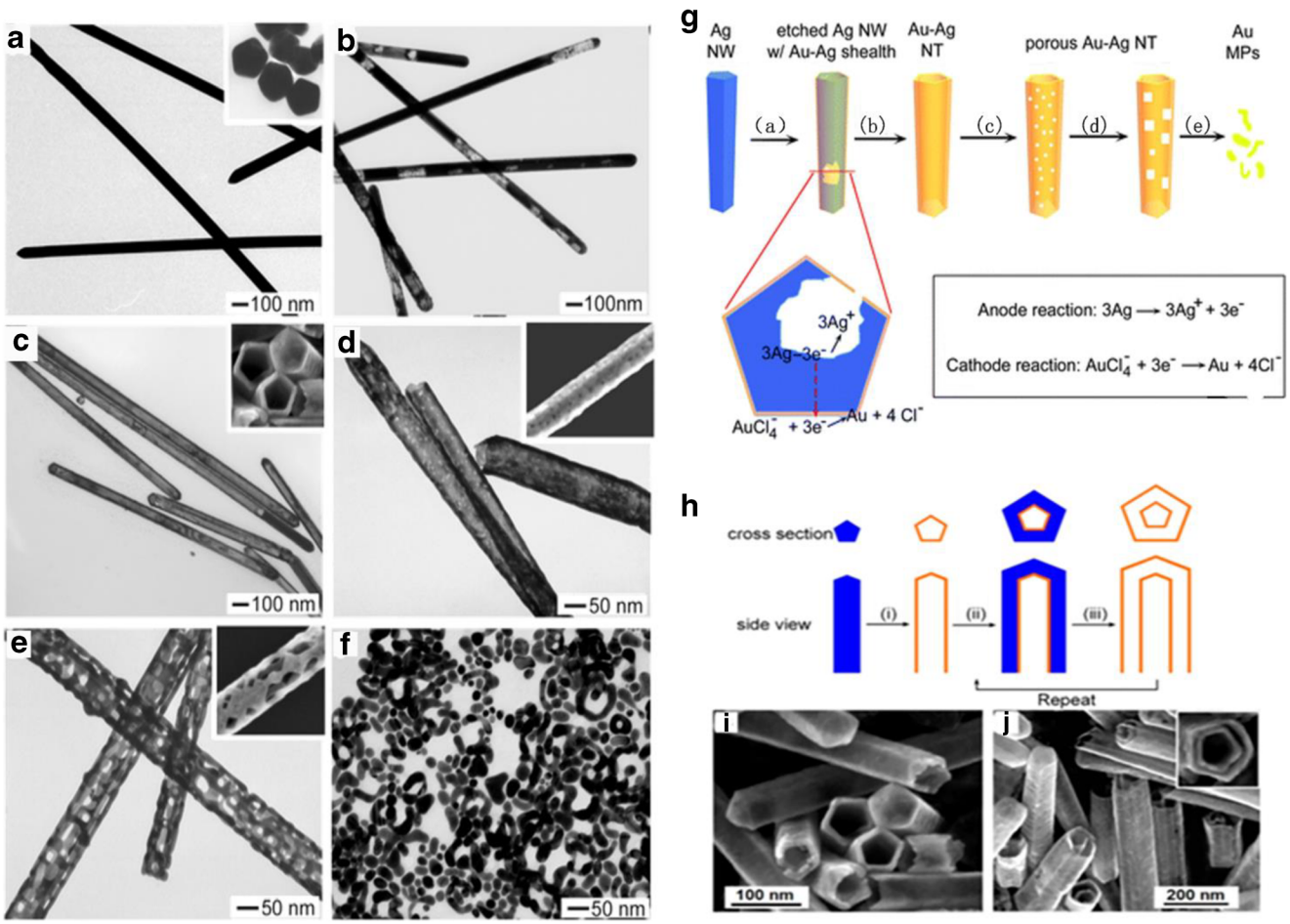

Fig. 3 **a** TEM images taken from Ag nanowires and **b**–**f** after they reacted with different volumes of 1 mM $HAuCl_4$ aqueous solution at 100 °C: **b** 0.3, **c** 0.6, **d** 1.5, **e** 2.3 and **f** 3.0 mL. **g** Schematic illustration the major steps involved in the galvanic reaction between Ag nanowires and $HAuCl_4$. NW, NT, and NPs represent nanowire, nanotube, and nanoparticles, respectively. Reprinted with permission from ref. [60]. Copyright 2010 Royal Society of Chemistry. **h** Chemical transformation of Ag nanowires to metal nanotubes with multiple walls through combination of galvanic displacement reaction and electroless plating of Ag. Reprinted with permission from ref. [50]. Copyright 2004 Wiley-VCH Verlag GmbH & Co. KGaA.Weinheim

solvothermal method, which is presented schematically in Fig. 4d. Ag nanowires exhibited a major peak around 405 nm originated from the transverse mode of SPR, after reacting with $HAuCl_4$, the peak of Ag NWs disappeared. AuAg alloyed nanotubes (AuAg ANTs) transformed by Ag NWs exhibited a major absorption centered at around 675 nm and a weak shoulder at around 550 nm. After the coating of CdS, the longer peak displayed a wide absorption and red-shifted to 805 nm (Fig. 4b) [64].

Most semiconductors have weak interactions with the visible light because of their small optical cross sections. Semiconductor coating is expected to generate a protective layer to prevent the metal from corrosion or oxidation. On the contrary, the presence of metallic ingredients may increase light-harvesting efficiency or photocatalytic by improving the charge separation at the metal-semiconductor interfaces and enhancing the light absorption [65]. Semiconductor nanostructures can be used to detect volatile organic compounds, so metal-semiconductor interface is expected to be actively explored for the detection of a variety of compounds. Moreover, the sensitivity, selectivity, and operational conditions of the sensors prepared by AuNTs/semiconductor materials could all be greatly improved, while enhancing its properties and applications.

According to the synthesis methods of gold nanotubes described above, including the hard template method and sacrificial template method. We found that the hard template method mainly used for synthesizing gold nanotube arrays by physical or chemical growth or deposition of nanomaterials into nanopores of the template. The morphology of AuNTs synthesized by hard template can be controlled according to TeMs thickness and the deposition time or PH. However, for the sacrificial template method, we mainly introduced the synthesis of gold nanotubes by galvanic replacement. The factors that may affect the morphology of gold nanotubes including precursor template, temperature, capping agent, reactant concentration

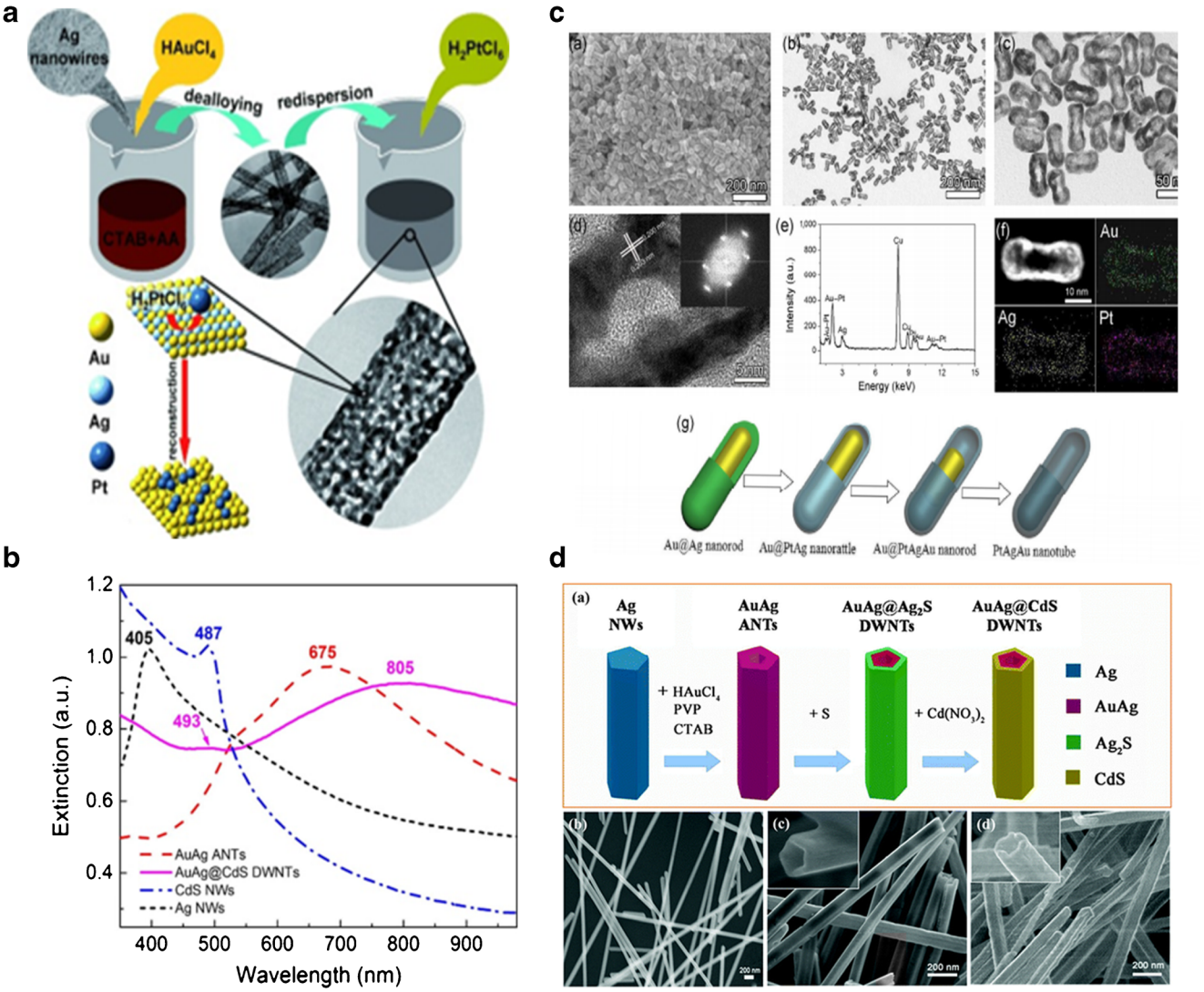

Fig. 4 **a** Preparation procedure of Pt/Au PNTs. Reprinted with permission from ref. [61]. Copyright 2010 Wiley-VCH Verlag GmbH & Co. KGaA, Weinheim. **b** UV-vis-NIR extinction spectra of the Ag NWs, AuAg ANTs, AuAg@CdS DWNTs and CdS NWs (dispersed in ethanol). Reprinted with permission from ref. [64] Copyright 2017 Elsevier B.V. **c** (a) SEM image; (b) and (c) TEM images; (d) HRTEM image; (e) EDS spectra of PtAgAu nanotubes. The inset of **(d)** is the SAED pattern. **(f)** HAADF STEM image of a single nanorod and the corresponding elemental maps. **(g)** cartoon of the product at different times during the formation of the PtAgAu hollow nanotubes. Reprinted with permission from ref. [62]. Copyright 2016 Springer Nature. **d** (a) Schematic of the procedure for preparing the AuAg@CdS DWNTs. typical SEM images of **(b)** Ag NWs, **(c)** AuAg ANTs and **(d)** AuAg@CdS DWNTs. Reprinted with permission from ref. [63]. Copyright 2017 Royal Society of Chemistry

etc. Table 1 illustrates the comparison between the two synthesis methods. The hard template method has a great advantage in the adjustable pore structure and morphology. The samples prepared by this method have good dispersion and uniform pore diameter, but the hard template method also has the disadvantages that partially filled samples discontinuous structure defects in the pores. The limited sources of template materials restrict the wide use of the hard template method. On the other hand, there are different types of sacrificial template materials. The sacrificial template method has the advantages of mass production, and equipment simply, good reproducibility during the process of synthesis. However, the sacrificial template method has also some disadvantages. The precursor itself must be capable to form a polymer structure with certain mechanical strength to ensure that the structure will not collapse after the removal of the template.

Despite the impressive development of AuNTs, there are still some challenges in further realizing its use in practical applications. For example, how to scale up the synthesis of AuNTs? To date, gold nanotubes have been prepared using the template methods, which means that the production is somewhat determined by the production of templates and mild reaction conditions. The use of the hard template–assisted electrodeposition method to realize large-scale synthesis is

Table 1 Comparison of sacrificing template method and hard template method

Methods	Hard template	Sacrificial templates
Template	AAO template/TeMs	AgNWs/AgNTs/MgO NWs
Mechanism of action	Physical or chemical growth or deposition	Galvanic replacement
Factors affecting Morphology	(1) Deposit time (2) Deposit temperature (3) TeMs thickness	(1) Precursor template (2) The amount of $HAuCl_4$ (3) Surfactant (4) Reaction time (5) Reaction temperature
Advantages	(1) Good dispersion (2) Uniform pore size	(1) Easier to build and remove than the hard template (2) Good reproducibility (3) Mass production
Disadvantages	(1) Easily cause damage to the structure of nanotubes (2) Sample only shows order for smaller particle size (3) Limited sources of template material	(1) The precursor itself must be able to form a polymer structure with mechanical strength
Mainly used to prepared style	AuNTs array	Various sizes, sharp structure of AuNTs

difficult due to the limited electrode area and the extra template removal steps required. For sacrificial template methods, although the frequently used templates, Cu and Ag nanowires can be synthesized on a large scale; a high temperature is usually needed. This requires the exploration of more facile methods to prepare these templates. Therefore, the lack of high-quality and large-quantity production methods for desired catalysts limits their commercialization. However, we believe that research on gold nanotubes will continue to expand in terms of synthesis methods and stability mechanisms to meet practical application needs in the foreseeable future. We also needed to combine theoretical research with practical applications more, not only to explore its synthesis mechanism but also to achieve the establishment of a large number of gold nanotube synthesis methods with good performance.

Factors affecting morphology

Precursor template

Generally, the morphology of gold nanotubes determined by the precursor template, such as length and wall thickness. To date, the most common precursor templates for the synthesis of gold nanotubes by galvanic replacement reaction are silver nanowires or nanorods, while the polyol method has been successfully synthesized Ag nanowires in many laboratories. Xia's team first pointed out that the change in the quality of silver nanowires is related to the purity of the chemicals used in the synthesis. Quantitative analysis shows that the main impurities Fe and Cl in ethylene glycol will affect the yield and quality of Ag nanowires with different batches [66]. However, a comprehensive understanding of the effects of impurities (i.e. Fe and Cl species) has also aroused researchers' interest in the effect of ionic additives on the morphology of silver nanoparticles and opened up a new way for shape-controlled synthesis of metal nanoparticles.

In another study, Ye's group [15] synthesized silver nanorods of controlled length, which were further prepared AuNTs over the range of 300–700 nm. The length of silver nanorods can be controlled by the number of seeds and growth temperature. It was found that the length of AgNRs varied inversely with seed amount and non-monotonically as a function of temperature. The growth rate of AgNRs accelerated with the increase in temperature, which leads to more disorder. The combined role of temperature and seed amount on AgNRs length was shown in Fig. 5a–e. In addition, the author reported that the absorption peak red-shifts with the increase in the length of gold nanotubes but the transverse mode is not sensitive to NT length. Furthermore, when a thin layer of Ag was coated on the nanotube through reduction and used as precursor templates, followed by another round of galvanic replacement with $HAuCl_4$, resulting in the formation of double-walled nanotubes. Repeating this cycle once, yielded more triple-walled Au-Ag nanotubes [50].

Raw material

As shown in Fig. 3g, with the increase in $HAuCl_4$, the silver nanowires are gradually etched into gold-silver bimetallic nanotubes with different morphology. Au-Ag bimetallic nanotubes also lead to the formation of needles on the surface, and the pore size depends to a certain extent on the volume of

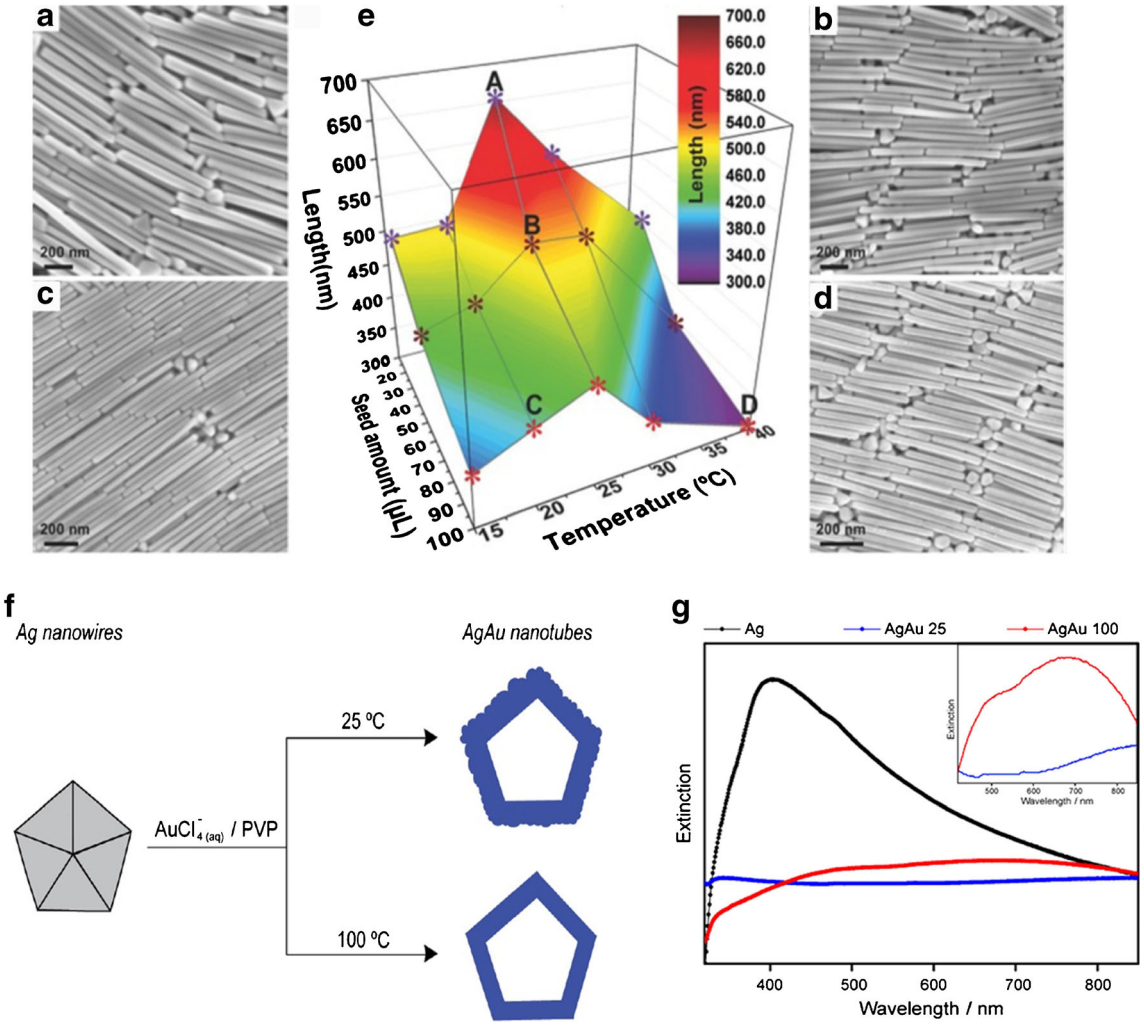

Fig. 5 **a**–**e** SEM images of Ag nanorods synthesized at 25 °C with different seed amounts, the number in brackets refer to the mean length and standard deviation; **a** 20 μL (670 ± 179) nm; **b** 50 μL (533 ± 126) nm. SEM images of AgNRs synthesized with 100 μL seeds at different temperatures **c** 20 °C (429 ± 116) nm; **d** 40 °C (305 ± 78) nm. **e** The length of Ag NRs as a function of seed amount and growth temperature. All the lengths were determined by examining SEM images of the resultant Ag NRs and represent the average (and the variance) of 300 NRs. (Scale bar = 200 nm). Reprinted with permission from ref. [15]. Copyright 2015 WILEY-VCH Verlag GmbH & Co. KGaA, Weinheim. **f** Approach for the synthesis of AgAu nanotubes displaying controlled surface morphologies by galvanic replacement reaction between Ag nanowires and $AuCl_4$ (aq) in the presence of PVP at different temperatures 25 °C and 100 °C. **g** UV-Vis extinction spectra recorded from aqueous suspensions containing Ag nanowires (black trace), AgAu 25 (blue trace), and AgAu 100 (red trace) nanotubes. The inset depicts a zoom in the 430–850-nm range for AgAu and AgAu 100 nanotubes (colour figure online). Reprinted with permission from ref. [67]. Copyright 2017 Sociedade Brasileira de Quimica

chloroauric acid added to the Ag dispersion [68]. The corresponding spectrum can also be changed (Fig. 6). When Ag nanowires react with a small amount (< 0.6 mL) of $HAuCl_4$, Ag nanowires firstly exhibit a major peak around 380 nm originated from the transverse mode of SPR, the peak firstly red-shifts then blue-shifts, finally disappeared, implying that the Ag nanowires are completely transformed into nanotubes. And additional peak appeared in 600 nm firstly red-shifts then blue-shifts back to 655 nm, indicating that the wall thickness of the nanotube increases as the displacement reaction continues (Fig. 6a). When they react with $HAuCl_4$ solution more than 0.7 to 2 mL, the peak at longer wavelength keeps red-shift to 930 nm. At this time, the dealloying process occurs and some small pinholes are formed on the wall of the nanotube (Fig. 6 b and c). When the amount of $HAuCl_4$ is more than 2.3 mL, the peak at 520 nm occurred, due to the nanotubes collapsing into pure Au nanoparticles. Reacting with more $HAuCl_4$ (> 2.5 mL), eventually destroying all nanotubes to form Au nanoparticles. In this process, the SPR peak of nanotubes can be tuned in the range of 655 to 930 nm, and then collapse into gold nanoparticles with increasing of $HAuCl_4$. In another study, for AuNTs of ~ 370 nm length

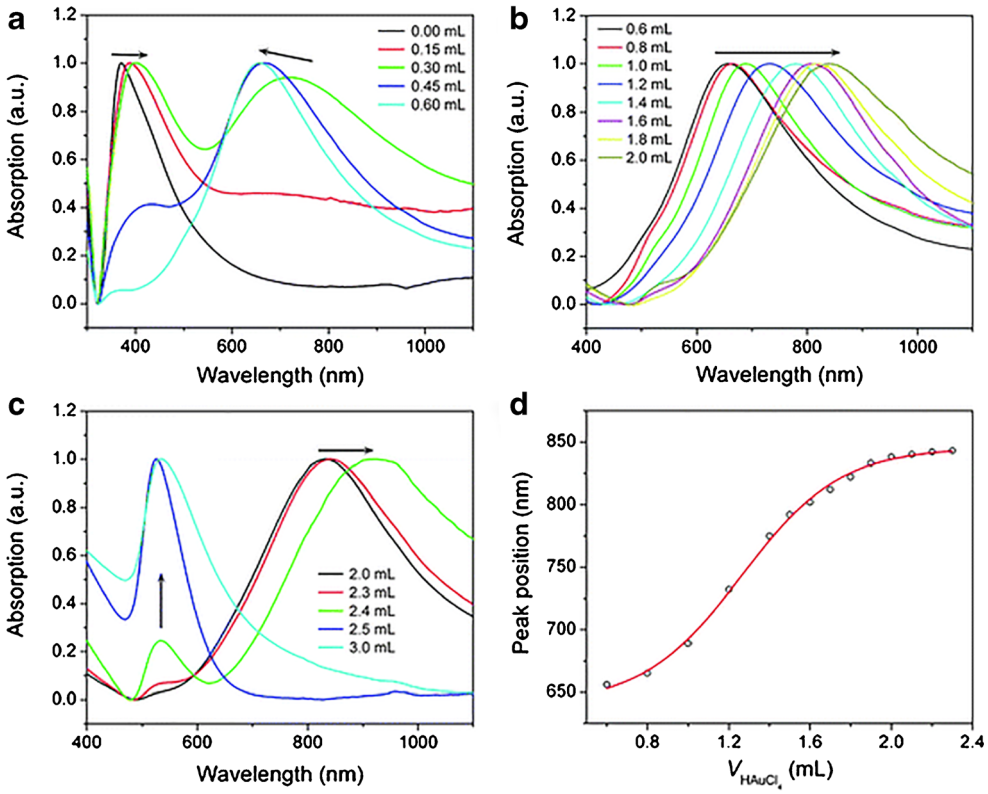

Fig. 6 **a**–**c** UV-visible-NIR absorption spectra of Ag nanowires (all in the same amount) before and after they reacted with different volumes of 1 mM $HAuCl_4$ aqueous solution. The numbers listed in each panel represent the volume of $HAuCl_4$ solution added to react with the Ag nanowires. All spectra were normalized against the intensities of the strongest peaks. **d** Absorption peak position of the nanotubes as a function of the volume of $HAuCl_4$ solution. Reprinted with permission from ref. [50]. Copyright 2004 WILEY-VCH Verlag GmbH & Co. KGaA.Weinheim

(Fig. 6), the peak tuned 775~880-nm range by changing $HAuCl_4$ amount from 20 to 50 μL [15]. Similar trends have been shown for Au nanocages [69], long Au nanotubes (of micrometres in length) [60]. Hunyadi et.al [56] made preformed silver nanowires in the seed-mediated growth method and used them as a sacrificial template to make silver-gold bimetallic nanoparticles that depended on the relative thickness of the metal, to ultimately hollow gold nanotubes. They reported that a variety of visible colours can occur in the visible with the increase in $AuCl_4^-$ ion. The Au nanotube diameter depends on the $AuCl_4^-$ ion concentration added to the system and increases when the $AuCl_4^-$ concentration increases.

In addition, some experimental studies have shown that the addition of reducing agents may affect the stability of the system. In the experiments of synthesizing Au-Ag alloy porous nanotubes, most of the Au atoms are deposited through the redox reaction between $HAuCl_4$ and reducing agent (such as ascorbic acid), when gold was solely produced via the galvanic replacement between $HAuCl_4$ and Ag nanowires, the system was unstable for the following two reasons: (i) a large amount of AgCl precipitate is formed, which further affects the reaction; (ii) when there is no other reduction in the case of an agent, when the volume of $HAuCl_4$ increases to more than 4 mL, the one-dimensional nanostructure decomposes into gold nanoparticles. On the contrary, when the reducing agent is added, even if the amount of $HAuCl_4$ is increased to more than 16 mL, the shape of the Ag nanowire template still retains well [70].

Temperature

Temperature is regarded as a key parameter in controlling the morphology of the AuNTs. By controlling the temperature of the galvanic substitution reaction between Ag nanowires and $AuCl_4^-$ (aq), the synthesis of AgAu nanotubes with smooth or branched surfaces was developed, which have been demonstrated by Xia [12, 50, 60, 71]. The diffusion rate of Ag and Au atoms is relatively high at 100 °C, and the uniform Au-Ag alloy is more stable than pure Au or Ag, so spontaneous alloying occurs between the deposited Au layer and the underlying Ag surface. Rodrigues et al. [67] found that Au/Ag nanotubes presented branched walls and surface plasmon resonance (SPR) band with low intensities in the visible were obtained at 25 °C. However, at 100 °C, the Au/Ag nanotubes presented smooth surfaces and SPR bands that closely matched the emission spectra of a commercial halogen-tungsten lamp (Fig. 5f, g).

Surfactant

As we all know, capping agents can change the surface energy of different facets of crystal nuclei and induce anisotropic growth. Silver nanowires synthesized by the polyol

method have a pentagonal cross section, five straight edges parallel to its long axis, five flat sides surrounded by [72] planes, ten {111} end faces and a five-fold symmetrical twin structure. In this process, the exposed faces of the decahedron of polytetragonal crystals are {111} faces with lower energy. Therefore, as long as the concentration of the precursor $AgNO_3$ is low enough, it will form a decahedron rather than a single crystal seed. Because the twin defect is the position with the highest energy in the seed, and it is also the position where the Ag atom tends to grow, the axis of the decahedron elongates and becomes a pentagonal rod, in which the side of the pentagonal rod is {100} crystal plane. When the pentagonal rod is formed, the PVP tends to adhere to the {100} crystal plane, that is to the side of the pentagonal rod, rather than to the end, which further leads to the formation of nanowires [11, 60]. In another study, Bi et al. [9] synthesized a large number of pentagonal gold nanotubes at room temperature by reducing chloroauric acid with silver nanowires in hexadecyltrimethylammonium bromide (CTAB) aqueous solution. They found that in the absence of CTAB, loose and hollow gold structures are usually prepared, and bundled gold nanotubes with rough surfaces can be obtained by replacing CTAB with polyvinylpyrrolidone (PVP) (Fig. 7a–d). The participation of CTAB is very important for the shape-controlled synthesis of pentagonal gold nanotubes. CTAB is not only an inducer to control the growth of gold nanotubes, but also a stabilizer for nanoparticles. There are Br^- ions in CTAB, which leads to the formation of AgBr precipitation in the displacement reaction at the same time. In the presence of AgBr, the interdiffusion rate between Ag and Au is greatly increased, which may lead to the heterogeneous structure of the product. Except for CTAB and PVP, 3,4-dihydroxyphenylalanine (DOPA) has been considered to be an efficient reducer and capping agent for the preparation of AuNTs at room temperature. Yang et al. [73] prepared caterpillar-like (CL) Au/Ag nanotubes and DOPA was used as a reducing and capping agent (Fig. 7e).

Reaction time

The incubation time also affects the morphology of gold nanotubes [9]. Yin et al. [74] prepared gold nanotubes with different morphology according to the different incubation times of precursor template and salt solution. The Ag nanowires are incubated with an aqueous solution of $Au(SCN)_4^-$, resulting in the galvanic substitution of silver and gold. The nanotubes were quantum matured in $Au(SCN)_4^-$ solution, then centrifuged at 1500 rpm for 5 min, the precipitates were collected, washed with ultra-pure deionized water for three times and finally re-dispersed in acetone. When the incubation time is 10 min, smooth gold nanotubes can be synthesized. When the incubation time is 24 h, rough porous gold nanotubes are formed (Fig. 7f, g).

Surface modification

Although gold nanomaterials have their unique advantages, there are also some disadvantages that hinder their applications. Nanomaterials have a high surface area and are easy to agglomerate, so they need to be modified to maintain their stability. There are many biocompatible polymers that can be capable of coupling to noble metal nanostructures, such as p(N-isopropylacrylamide), polydopamine [75], beta-cyclodextrin (β-CD) [76], aminothiols [77] and so on. The modified nanomaterials have a wide application prospect in the field of biomedicine. In addition, surface modification can greatly improve the biocompatibility. For instance, nanoparticles modified with hydrophobic organic ligands (such as oleic acid) cannot be straight used due to their poor hydrophilicity and lack of functional groups. In this respect, it is indispensable to chemically modify the surface of nanoparticles to make them hydrophilic and biocompatible. Ye et al. synthesized AuNTs modified by PSS (poly (sodium 4-styrenesulfonate)), which imparted colloid stability and low cytotoxicity [15]. PSS-AuNTs showed strong photoacoustic signal in vivo and accumulated in SW620 tumour, so it can be used as an effective photoacoustic imaging (PAI) contrast agent [15].

The surface modification of metal nanomaterials cannot only change the local dielectric environment of metal materials but also greatly affect their optical properties. In another study, Liu and co-workers [78] prepared cysteine-modified Au/Ag alloy nanotubes. By coupling cysteine with Au/Ag alloy nanotube, which produced a strong chiral response in the range from ultraviolet (UV) to visible spectrum. Compared with Ag- or Au-cysteine chiral hybrid nanorods, cysteine-modified Au/Ag nanotubes exhibit higher chiral responses due to stronger local electromagnetic fields. The reason is that the near-field enhancement effect of plasmonic nanotubes and the coupling between cysteine and Au/Ag ANTs induced by Coulomb interaction form an extended spiral network on the surface of Au/Ag ANTs (Fig. 8). Surface modification is an effective method to regulate the interaction between materials and cells, and even determine the functions and properties of materials in the life system. Because most nanoparticles are hydrophobic which is not suitable for clinical use.

Morphology, as an important parameter for characterization of material properties, together with length, specific surface area and pore structure, determines the properties of gold nanotubes, consequently, pinpoints their application. For the hard template method, the length of gold nanotubes is controlled by thickness of template. In addition, the deposition

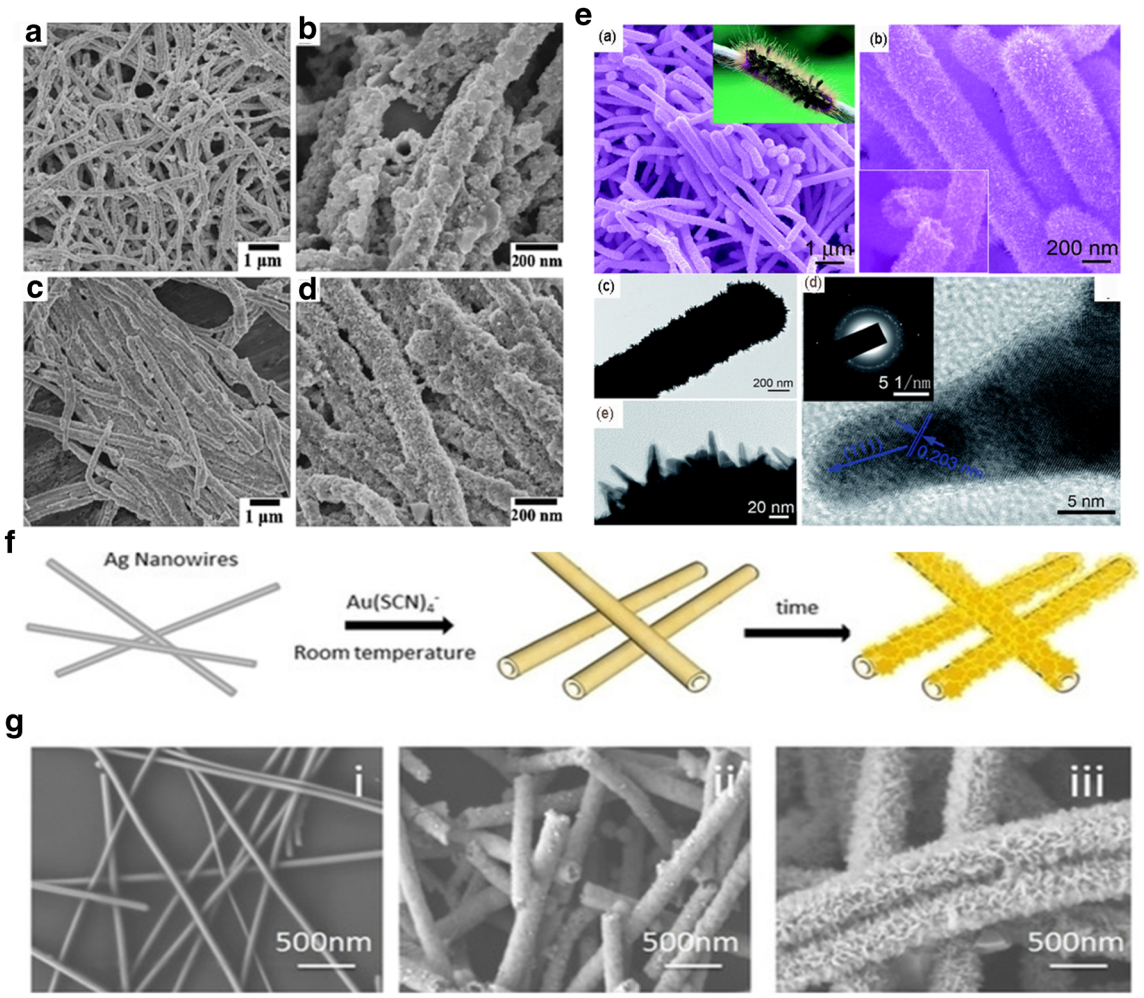

Fig. 7 **a** and **b** SEM and FE-SEM images of the gold nanotubes prepared in the absence of CTAB; **c** and **d** SEM and FE-SEM images of the gold nanotubes prepared in the presence of PVP. Reprinted with permission from ref. [9]. Copyright 2008 IOP science. **e** FE-SEM images of Ag wire (**a**), caterpillar-like Au nanotubes (**b**), CLGNs nanotubes (**c**) and XRD images of the as-prepared material (**d**, **e**), TEM image of Cu_2O-CLGNs. Reprinted with permission from ref. [73]. Copyright 2014 Royal Society of Chemistry. **f** Scheme depicting the synthesis process, starting from Ag NWs, which transform into porous Au nanotubes upon incubation with gold thiocyanate. **g** Scanning electron microscopy (SEM) images of the starting Ag NWs (i), Au nanotubes formed after 10 min of incubation with Au $(SCN)_4^-$ (ii), and 24 h of incubation (iii). Reprinted with permission from ref. [74]. Copyright 2017 WILEY-VCH Verlag GmbH & Co. KGaA.Weinheim

time, deposition potential and concentration of solution are also important factors to control the morphology of gold nanotubes [42]. For example, the inner diameter of gold nanotubes becomes smaller as depositing time increased on the AAO template. The length of nanotubes and the thickness of gold film decrease with the increase in plating temperature on TeMs [47]. For the sacrificial template method, the morphology of gold nanotube control mainly relies on the synthesis of the template under certain conditions. Additionally, the inner diameter of gold nanotubes is controlled by the amount of $HAuCl_4$. Capping agent is also regarded as a key factor. Table. 2 summarizes and compares the different functions of different factors in the morphology control. We can synthesize the gold nanotubes we need by controlling the parameters of the raw materials. For example, we can prepare gold nanotubes of different thickness and different porosity by controlling the volume of chloroauric acid and reducing agent; we can determine the length and diameter of gold nanotubes by controlling the length and diameter of the precursor template; capping agents are added to increase the stability of morphology.

Properties

Surface plasmon resonance

As we all know, the free electrons of precious metal nanomaterials can be regarded as a plasmon. The incident light illuminates the nanomaterial; the surface plasmon resonance (SPR) is formed when the collective oscillation frequency of the surface electrons matches the frequency of the

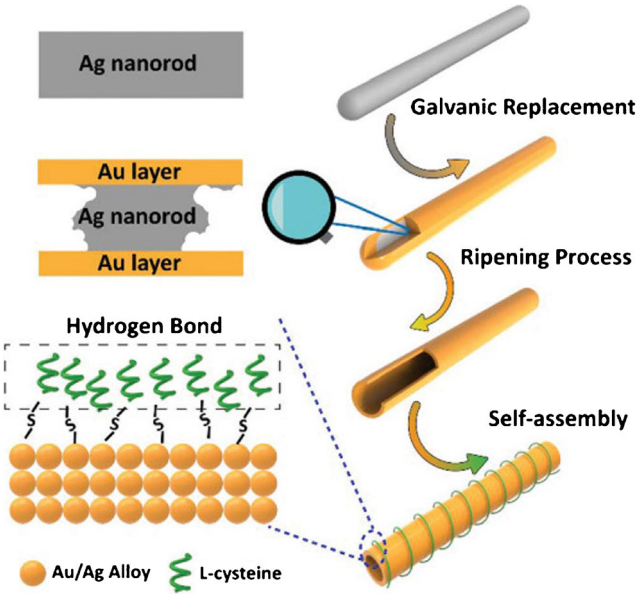

Fig. 8 Schematic illustration of the formation process for cysteine-modified Au/Ag ANTs. Reprinted with permission from ref. [78]. Copyright 2019 Royal Society of Chemistry

incident light. Gold nanoparticles have unique spectral properties because of the active SPR vibrational band, such as absorption and Rayleigh scattering. This resonance makes effective absorption, scattering and near-field enhancement possible; the frequencies depend on the size, shape and surrounding medium of nanoparticles. Gold nanotubes have rich optical properties due to their controllable structures, such as length, wall thickness, inner diameter and element composition etc.

Zhu et al. [79] found that light scattering of gold nanotubes is greatly affected by wall thickness. Reducing the wall thickness of gold nanotubes will lead to the decrease of plasmon band energy and the loss of surface electron coherence. The red-shift of light-scattering peak is nonlinear and broadened. For gold nanotubes, the effective average free path is equal to the length of the wall chord, which has an important effect on the scattering bandwidth. When the effective average free path is equal to the length of the golden wall chord, the full width at half maximum (FWHM) of the light scattering peak is inversely proportional to the effective mean free path. He also [14] studied theoretically the transverse surface plasmon resonance in Au-Ag alloy nanotubes by the Drude model and quasi-static approximation (Fig. 9a). He found that both symmetric and antisymmetric SPR in Au-Ag alloy nanotubes can be adjusted by changing the alloy composition and shell thickness. The symmetrical SPR led to red-shift in the infrared region by increasing the gold composition or decreasing the shell thickness (Fig. 9b). However, the antisymmetric SPR is more sensitive to the change of gold composition and only red-shift in the visible region. Due to the local electric field corresponding to the antisymmetric coupling is parallel to the incident polarization, the thin shell enhances the electron scattering and reduces the energy of the plasmon, resulting in a strong red-shift of the SPR. Murphy's team also found extinction peak of AuNTs becomes blue-shift and more absorbing with the wall thickness was increased by experimentally and finite element modelling (Fig. 9c, d). Both of their observations are in good agreement with the experimental findings. In addition, the extinction peaks of AuNTs showed red-shift with diameter in strength increasing (Fig. 9e, f) [31].

In another study, Zhao et al. found that the scattering spectra of dielectric Au-Ag double nanotubes have at most three pronounced resonance light-scattering (RLS) peaks in the visible region, which are respectively attributed to the antisymmetric

Table 2 Different factors affecting the morphology of gold nanotubes

	Hard template		Sacrificial template
	AAO	TeMs	
length	(1) Tailor the puttering conditions (2) AAO thickness	(1) Deposit temperature (2) TeMs thickness (3) Deposition potential (4) Solution concentration	(1) Precursor length
Wall thickness	(1) Polymer core hydrophobicity	(1) Pore diameter of template	(1) $HAuCl_4$ (2) Precursor
Inner diameter	(1) Deposition time	(1) Temperature	(1) $HAuCl_4$ (2) Precursor
Surface roughness	(1) Tailor the puttering conditions (2) AAO template (3) Electrodeposition approach	(1) Form of formwork removal	(1) Reaction temperature (2) Capping agents (3) Incubation time

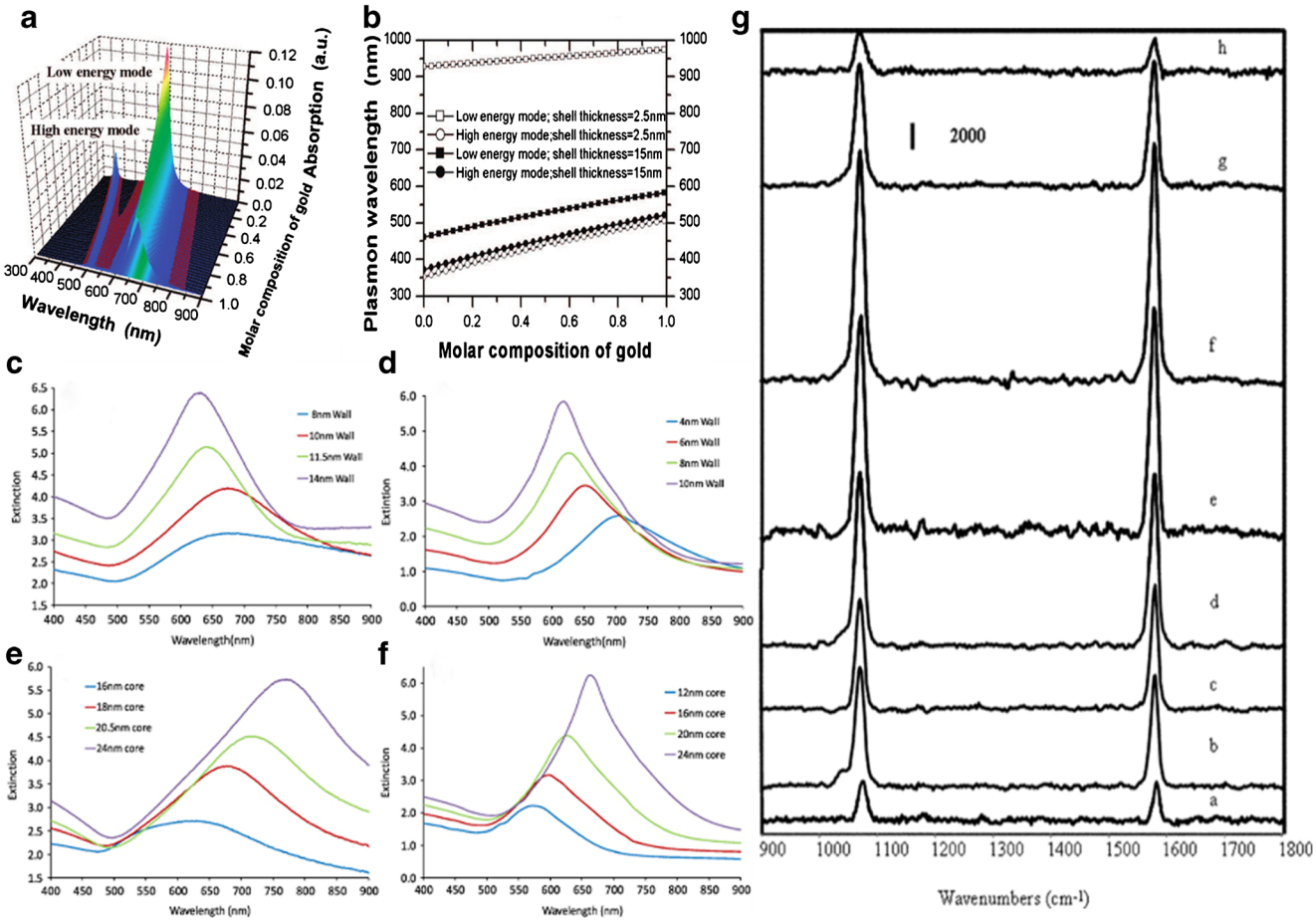

Fig. 9 Schematic for AuNTs absorption spectra. **a** Absorption spectra of Au-Ag alloy nanotube with different molar composition of gold, r1) 17.5 nm and r2) 25 nm. **b** Resonance wavelength of surface plasmon in Au-Ag alloy nanotube as a function of gold molar composition. Reprinted with permission from ref. [14]. Copyright 2009 American Chemical Society. **c** Measured and **d** simulated normal incidence ($\theta = 0°$) extinction (−Ln(T)) spectra of gold nanotube arrays with varying wall thickness. The nanotubes have constant inner diameters and lengths. **e** Measured and **f** simulated normal incidence ($\theta = 0°$) extinction (−Ln (T)) spectra of gold nanotube arrays with varying inner core diameters. The nanotubes have constant wall thicknesses and lengths. Reprinted with permission from ref. [32]. Copyright 2011 IOP science. **g** Surface-enhanced Raman spectra of 4-MBA using Au nanotubes with various shell thickness: (a) 9 ± 1 nm, (b) 11 ± 1 nm, (c) 13 ± 1 nm, (d) 16 ± 1 nm, (e) 18 ± 1 nm, (f) 21 ± 2 nm, (g) 25 ± 3 nm. Reprinted with permission from ref. [56]. Copyright 2006 Royal Society of Chemistry

plasmon coupling of the outer Ag wall, the symmetric coupling of the inner Au wall and the cavity plasmon on the inner surface of Au wall [80]. The outer dielectric surrounding has a great influence on the intensity and wavelength position of the RLS. The longest wavelength RLS (Peak 3) is always enhanced with the increase in outer surrounding dielectric constant, i.e.ε_4. When the thickness of the Ag coating is much smaller than that of the Au wall, the change of ε_4-dependent scattering intensity of mid-wavelength RLS becomes non-monotonic. On the contrary, when the thickness of Ag coating is much larger than that of the Au wall, the change of RLS scattering intensity dependent on ε_4 becomes non-monotonic at a shorter wavelength. The number of RLS bands can be fine-tuned by changing the dielectric constant of the inner dielectric wire. Velichko and coworkers [81] studied the scattering and absorption of H-polarized light by circular gold nanotubes and found that the second quadrupole resonance peak appears in the absorption spectrum when the thickness of gold nanotubes is less than 5 nm. This kind of quadrupole hybrid plasmon resonance has a larger value of quality factor and is more likely to be used to the sensing of the refractive index changes of the host medium than dipole resonance. By studying the coaxial gold nanotubes, Xu's team [82] found that the transmission spectrum can be controlled by adjusting the thickness and spacing of the nanotubes and the dielectric constant between the inner and outer nanotubes. The formant near the left band gap is closely related to the dielectric constant, the distance between the two tubes and the thickness of the inner and outer tubes.

The surface plasmon resonance of gold nanotubes relies sensitively on the nanoparticle geometry and its environment. The shape of Au nanotubes is an important parameter in governing their properties. Their SPR properties can be tailored by synthetically tuning their sizes, shapes and composition. Compared with other nanocrystals, Au

nanotubes provide significant advantages in this aspect. The optical properties of gold nanotubes are controlled by many factors, such as length, wall thickness and the ratio of gold composition, etc. Gold nanotubes with symmetry usually exhibit two plasmon modes. One is the longitudinal SPR mode associated with the electron oscillations along the length axis, and the other is the transverse SPR mode excited by light polarized along the transverse direction of the nanotube. The plasmon wavelength of the longitudinal mode can be synthetically tuned across a wide spectral range, covering the visible and near-infrared regions by adjusting its length or gold composition. For example, the absorption peak red-shifts with the increase in the length of gold nanotubes but the transverse mode is not sensitive to NT length. In addition, symmetric and antisymmetric SPR in Au-Ag alloy nanotubes can be tuned by changing the alloy composition and shell thickness. The symmetrical SPR led to red-shift in the infrared region by increasing the gold composition or decreasing the shell thickness.

Surface-enhanced Raman scattering

Surface-enhanced Raman scattering (SERS) spectroscopy can uniquely identify the structure information of molecular and have been extensively applied in molecular detection, so more and more researchers are interested in it. Gold nanotube provides more sites for analyte adsorption because of increasing surface area compared with solid equivalents [19]. This indicates that nanotube provides an additional advantage for measuring low concentrations of analyte by SERS. Hunyadi et al. [56] compared the surface-enhanced Raman spectra of 4-MBA on silver nanowires, silver-gold bimetallic nanowires and gold nanotubes, and calculated their enhancement factors (Fig. 9g). They found the enhancement factors are 6 to 7 orders of magnitude compared with the analyte alone and a intermediate amount of Au gave the best SERS enhancement. Bimetallic nanowires provided more SERS signals than Ag nanowires and a factor of 40 at best, 5 at the least. Gold nanotubes are better than solid gold nanorods in similar colloidal SERS experiments. In another study, Yang et al. [-73]studied the SERS signals at different sites on a single caterpillar-like Au/Ag NTs by R6G molecules as the adsorbate and found that surface enhancement factors of the NTs with and without spines were around 10^5 and 10^4 respectively, which can be attributed to induce the antenna effects on the entire surface of the NTs. Costa's research [83] reported that the SERS properties of the Ag-Au NTs displayed more superior relative to Ag NWs and are enable to the detection crystal violet in the 10^{-10} M regime, as well as 9-nitroanthracene and benzo[α]pyrene at 3.3×10^{-7} M.

SERS can detect the molecules of interest with low abundance quickly and reliably because it can generate many orders of magnitude enhanced Raman signals on the surface of adsorbed molecules. The SERS sensitivity largely relied on electromagnetic "hotspots" where local electric field is fairly intense. In addition, it is important to mention that molecules must be located close to the surface of the Ag or Au nanostructures for the SERS effect to take place in the visible range, according to the electromagnetic mechanism of enhancement. Compared with solid gold counterparts, porous gold nanotubes generated more hot spots the increase in specific surface area, which were responsible for a higher SERS performance. Furthermore, the 124-fold increase in the area of the CV band at 1172 cm^{-1} relative to Ag NWs was estimated assuming that each Ag NW was converted to a Ag-Au NT during the synthesis [83].

Catalytic properties

AuNTs are characterized by large surface-to-volume ratio, high porosity, open tube structures and more active sites, which are available for more target molecules compared with solid counterparts. Thus, gold nanotubes can further enhance electrochemical characteristics, improve capability of catalyst and high faradaic current density so that become a promising candidate for preparation of sensitive modified electrodes [45]. Recently, a variety of electrode modified electrocatalysts (AuNTs) have been used as microelectrodes and probes and for the determination of electrochemically active compounds [34–36]. Mashentseva et al. compared the catalytic activity of PET track-etched membranes embedded with silver and gold nanotubes. The result found Ag/PET composites rate constant was enhanced with increasing temperature and the activation energy 42.13 kJ/mol. More powerful catalytic activity was demonstrated for Au/PET composites [16]. Gu and coworkers synthesized platinum-decorated Au porous nanotubes, which mitigate the "poisoning effect" of Pt suffered from CO-like species generated during the electrochemical process [61]. In Sun's research, PtAgAu nanotubes exhibited good catalytic activity in the electrooxidation reaction of formic acid [62].

Biomedical application

Biosensing

Biosensors consist of a biological recognition element, generally called the bioreceptor, the transducer component, and the electronic system (often combined with the transducer). Depending on the bioreceptor type used, biosensors can broadly be classified into four classes: nucleic acid/DNA, enzymes, antibody-antigen and cells. One of the major roles of gold nanotube as sensors is to detect

biomarkers and improve the sensitivity and accuracy of diagnosis. Many researches have indicated that gold nanotube has a larger surface area, faster electron transfer rate, more active sites and easier immobilization for enzyme; AuNTs have a wide application in biosensors such as DNA sensor, immunosensors, enzyme sensor, aptasensors and so on [84]. The relevant literatures of AuNTs' application in the field of sensing are summarized in Table 3. According to the current literature on the application of gold nanotubes in biosensing, we mainly introduce DNA sensors, immunosensor, protein sensor and some other gold nanotube-related sensing applications.

DNA sensors

Deoxyribonucleic acid (DNA) is a two-chain molecule that carries genetic information about the development, growth and reproduction of all known organisms and many viruses. DNA can be important biomarkers of disease diagnosis [85]. Traditionally, the technology of PCR detection of DNA has the characteristics of complexity, easy pollution, high cost and lack of portability, while the rapid, simple, cheap and quantitative sensor detection of specific genes has a huge potential market [86]. Tuberculosis is a common infectious disease caused by *Mycobacterium tuberculosis* [87]. In general,

Table 3 An overview on AuNT-based biosensors, with data on analytes, methods and LOD

No.	Analyte	Features	Ref.
1	HCG	PC membrane + electrodepositing; immunosensor Linear range, 25~400 mIU/ml; LOD, 12 mIU/ml	[48]
2	HCG	AAO template + electrodeposition; immunosensor Linear range, 0.1~100 $mIUmL^{-1}$; LOD, 0.08 mIU/mL	[34]
3	Morphine	AAO template + electrodeposition; electrochemical sensor Linear range, 1.22×10^{-7}~7.44×10^{-4} mol/L; LOD, 4.06×10^{-8} mol/L	[35]
4	AA and UA	AAO template and PC membrane; electrochemical sensor AA: linear range, 1.02×10^{-7}-5.23×10^{-4} $molL^{-1}$; LOD, 1.12×10^{-8} mol/L UA: linear range, 1.43×10^{-7}–4.64×10^{-4} mol/L; LOD, 2.24×10^{-8} mol/L	[36]
5	AA	Replacement reaction with AgNWs templates; electrochemical sensor Linear range, 5~2000 μM; LOD, 2 μM	[3]
6	Glucose	Replacement reaction with AgNWs templates; nonenzymatic glucose electrochemical biosensors Linear range, 0.1–5 mM; LOD, 1.83 μM	[18]
7	Glucose	AAO template + electrodeposition; electrochemical sensor Linear range, 5 μM~16.4 mM; LOD, 2.1 μM	[33]
9	*Mycobacterium tuberculosis* DNA	PC membrane + electrodepositing; electrochemical DNA biosensor Linear range: 0.01~100 ng/mL; LOD: 0.05 ng/μL	[88]
10	aflatoxin B1	track-etched polycarbonate membrane; electrochemical immunoassay Linear range: 4×10^{-12}~6×10^{-9} g/mL; LOD:1×10^{-12} g/mL	[89]
11	PRRSV	TeNWs templates; electrochemical immunoassay; Linear range: $1:10^3$~$1:10^6$ (dilution ratio); LOD: 10.8 pg/mL	[76]
12	HPV	PC membrane + electrodepositing; electrochemical DNA biosensor. Linear range: 0.01 pM~1 mM; LOD: 1 fM	[37]
13	Biotin/streptavidin; immunoglobulin; ricin protein antibody	PET membrane + deposition; Molecular recognition and specific interaction Immunoglobulin: Linear range: 10–100 nM	[49]

HCG: human serum chorionic gonadotrophin; *PC*: nanopore polycarbonate; *AA*: ascorbic acid; *UA*: uric acid; *PRRSV*: porcine reproductive and respiratory syndrome virus; *HPV*: human papilloma virus; *PET*: poly (ethylene terephthalate) membrane

diagnostic methods for TB include polymerase chain reaction (PCR), immunoassay and Southern hybridization. However, these methods are commonly expensive, time-consuming and limited in the use of hazardous materials.

Many researches have demonstrated that the ordered, rough porous modified and other electrodes with high surface areas can enhance electrochemical characteristics. Compared with nanowire array electrode and nanorod electrodes, highly ordered gold nanotube array electrodes have outstanding ability to improve capability of catalyst and signal-to-noise ratio due to their hollow nanostructures which can provide more surface and electroactive sites. Torati et al. [88] developed a gold nanotube array (AuNTsA) with a length of about 1.5 μm and a diameter of about 200 nm by template-assisted electrochemical deposition technology (Fig. 10a). They found that AuNTsA had better electron transfer surface than bare Au electrode. Therefore, DNA hybridization biosensor was prepared for detection of *Mycobacterium tuberculosis* DNA using AuNTsA as electrode. The biosensor has a good linear range of 0.01~100 ng/μL and 0.05 ng/μL as the detection limit. Human papilloma virus is a type of human papillomavirus (HPV). Cancer caused by HPV infection is the second leading cause of cancer deterioration in women in developing countries and one of the leading causes of death worldwide. Shariati's group [37] designed an impedance human papilloma virus (HPV) DNA biosensor by covalently immobilizing single-stranded DNA (ss-DNA) probe on AuNT-PC electrode without labelling detection (Fig. 10b). The AuNTs decorated PC not only amplify the electrochemical impedance spectroscopy (EIS) signal under applied electrical field but also enhance the detection sensitivity to the HPV DNA sequences because of high sensitivity of the AuNTs surface. Meanwhile, the biosensor can distinguish complementary, mismatched and non-complementary DNA sequences, which

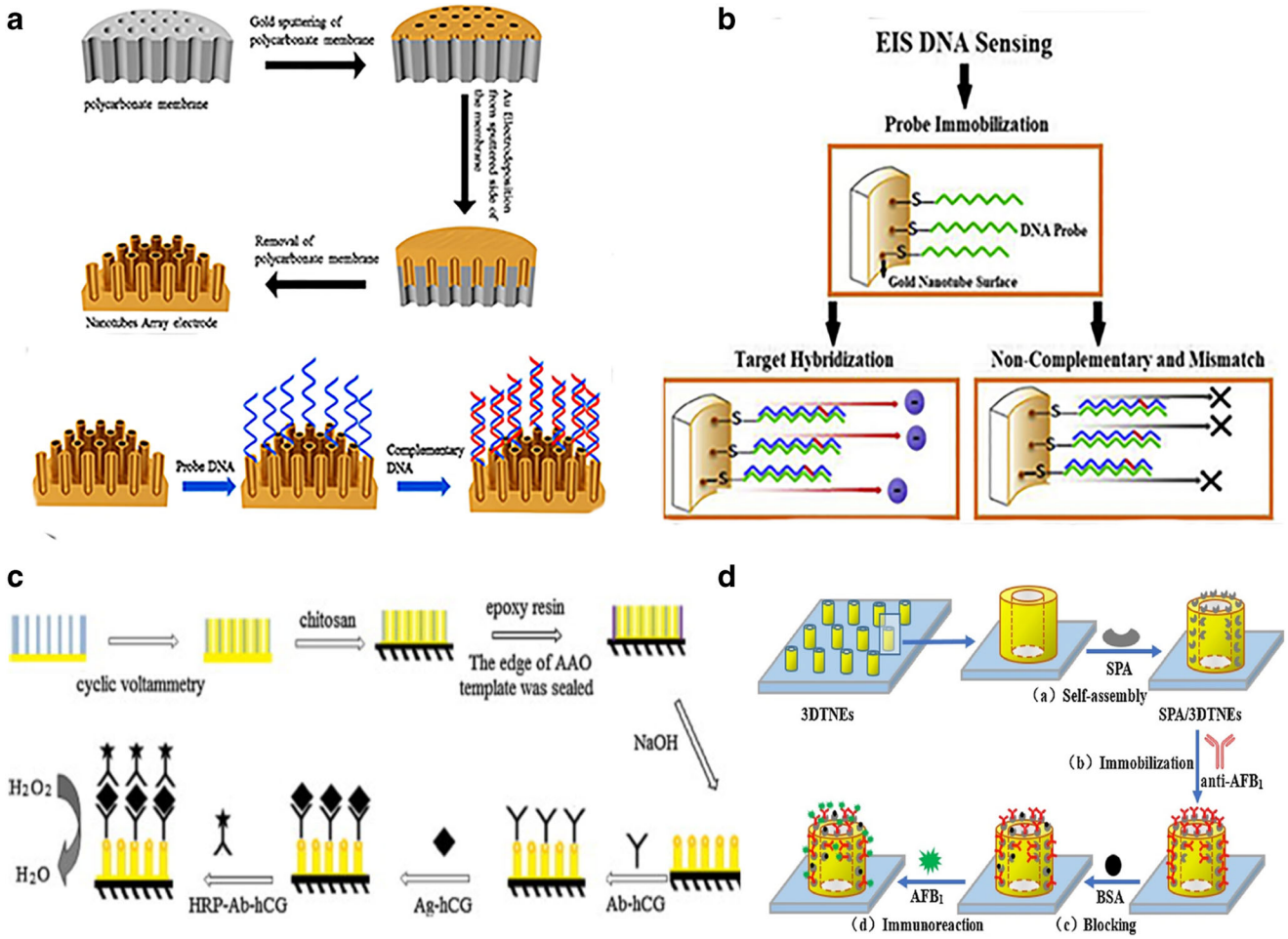

Fig. 10 **a** Schematic drawing of Synthesis of AuNTsA and fabrication of the DNA hybridization biosensor based on AuNTsA electrodes. (WE—working electrode, RE—reference electrode, CE—counter electrode). Reprinted with permission from ref. [88]. Copyright 2015 Elsevier B.V. **b** The modifications of the AuNTs surface. The schematic image for probe immobilization and hybridization of the HPV DNA target sequences on the AuNTs PC surface. Reprinted with permission from ref. [37]. Copyright 2019 Elsevier B.V. **c** The schematic diagram of the stepwise procedure of the immunosensor. Reprinted with permission from ref. [34]. Copyright 2011 IOP science. **d** Schematic diagram of the stepwise fabrication process of the immunosensor. Reprinted with permission from ref. [89]. Copyright 2017 Elsevier B.V

can detect human papilloma virus with high selectivity, low limit of detection (LOD) of 1 fM and widely linear range at 0.01 pM~1 mM.

Immunosensors

The level of human chorionic gonadotropin (HCG) in serum or urine has become an important biomarker for the diagnosis of early pregnancy and many diseases related to the seminal system, such as orchic teratoma and the trophoblastic carcinoma. Metallic alloy nanomaterials often present better catalytic properties than monometallic counterparts. Au has low reactivity and favourable biocompatibility compared with platinum, which can be used to immobilize biomolecules. Au-Pt alloys may have unique effects on catalysis, optical properties, selective oxidation and selective sensors. Tao et al. [48] synthesized Pt-Au alloy nanotube array with polycarbonate (PC) template by means of direct electrodeposition technique at − 0.35 V. The immunosensor was based on the obstruction of HCG antigen to the electrocatalytic reduction of H_2O_2 by Pt-Au alloy after binding to the surface of electrode through immunoreactions, which can detect the concentration of HCG ranging from 25 to 400 mIU/mL and low limit of detection at 12 mIU/mL. Similarly, the author's group [34] also designed an amperometric immunosensor for determination of HCG by immobilizing HCG antibody onto gold nanotube array (Fig. 10c). The immunosensor can detect human chorionic gonadotropin in serum samples with satisfactory regeneration, stability and selectivity, low limit of detection (LOD) of 0.08 mIU mL^{-1} and widely linear range at 0.1 to 100 mIU mL^{-1}. In another study, Fig. 10d, Li and co-workers developed a type of immunosensor based on orientated staphylococcus protein A (SPA) modified gold three-dimensional nanotube ensembles (3DTNEEs), which was detected aflatoxin B1(AFB1) [89]. The detection concentration of AFB_1 linear range from 4×10^{-12} to 6×10^{-9} g/mL and low limit of detection at 1.0×10^{-12} g/mL.

Protein biosensors

There are many methods for protein quantification, such as the Kjeldahl method, near-infrared spectroscopy, ultraviolet absorption method, Biuret method, etc. In recent years, new protein detection methods have been developed, such as biosensors. The biosensor has great advantages because of its fast, cost, simplicity, portability and easy mass production. In particular, nanomaterials maximize improved the performance of protein biosensors by nanomaterials interact with specific proteins. Nanomaterials have been the driving force for the development of precision biosensors in recent years. The use of metal nanoparticles has been widely observed in the literature, such as Au and Pt [84, 90]. Au has good biocompatibility to protein, which can be used to immobilize biomolecules. The ion current Conical gold nanotube can be orders of magnitude higher than that in a cylindrical tube/pore of the same diameter. The protein analyte can bind to a biochemical molecular recognition agent immobilized at the small diameter opening of the conical nanotube and be detected. Sexton et al. [91] prepared poly (ethylene glycol) (PEG)-functionalized conical gold nanotube in poly (ethylene terephthalate) (PET) membrane by track etching (Fig. 11a, b). The nanotube current pulse sensors can be used to detect protein analytes and that selectivity can be obtained by adding antibodies to the target protein to the analyte solution. In another study, Siwy and co-workers developed a new type of protein biosensor that the protein analyte is combined with a biochemical molecular recognizer fixed to a small diameter (5~9 nm) opening of a conical nanotube [49]. The biosensor is based on a single conical AuNTs embedded within a mechanical and chemically robust polymeric membrane. Finally, the author detected three different molecular recognition agents in this sensor: biotin/streptavidin [92], protein-G/immunoglobulin (IgG) [93] and an antibody to the protein ricin [94] as the MRA and ricin.

Other biosensors

There are other examples of gold nanotubes used as electrodes to detect other biomolecules due to their excellent catalytic properties. For instance, Yang and co-workers synthesized gold nanotube arrays (using AAO) during short time and fabricated an electrochemical sensor for determination of morphine [35]. Furthermore, they simultaneously detected ascorbic acid (AA) and uric acid (UA) in real human urine and serum samples with satisfying results by differential pulse voltammetry in this sensor [36]. Tian et al. [33] found that Au-NTA electrode exhibit better electrocatalytic activity than Au-NW. Au-NTAs were grown in alumina oxide templates by galvanostatic deposition and utilized for glucose determination in serum samples. The linear range from 5 μM to 16.4 mM glucose concentration, the sensitivity of 44.2 μAmm^{-1} cm^{-2} and the detection limit of 2.1 μM.

In a word, biosensors have been classified according to the bioreceptor type above. In addition, we need to note that aptamer-based sensors have been the research hotspot in recent years. An aptasensor is a particular class of biosensor where the biological recognition element is a DNA or RNA aptamer. Aptamers are favourably used in biosensors as sensitive and selective bioreceptors coupled with a variety of transducer principles such as optical, mass-sensitive and electrochemical detection. The analytes cover a wide range from small molecules, like nucleotides, cofactors, amino acids, organic molecules over peptides, polysaccharides and proteins, to complex structures like whole cells, viruses and single-cell organisms [95]. The aptamer biosensor not only has strong specificity but also improves sensitivity. The unique and strong host-guest recognition between cyclodextrin and

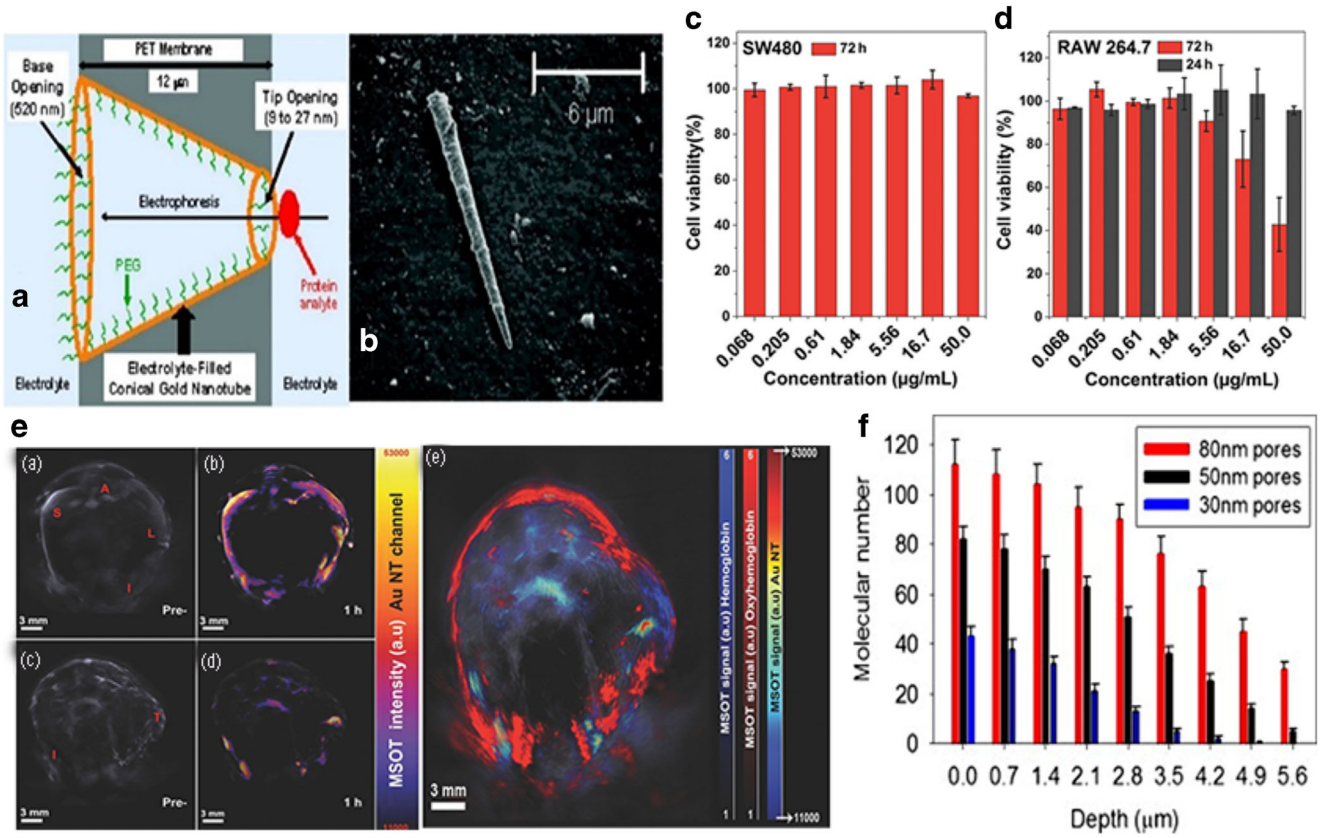

Fig. 11 **a** Schematic of the PEG-functionalized conical gold nanotube sensor element, showing the base-opening and tip-opening diameters used in these studies. Not to scale. **b** Electron micrograph of such a sensor element after removal from the PET membrane. Note that in the sensing experiment, the nanotube is left embedded in the PET membrane, but it was removed here so that it could be imaged. Reprinted with permission from ref. [91]. Copyright 2007 American Chemical Society. **c**, **d** In vitro cell viability of SW480 cells and RAW 264.7 cells with increasing concentrations of PSS-coated Au NTs (~ 370 nm in length, Au mass fraction = 73.9%). Results are shown as mean ± SD ($n = 3$) as determined using CCK-8 assays [15]. **e** In vivo non-background-corrected orthogonal images of HCT tumour-bearing mice at varied time points after tail-vein injection of PSS-Au NTs. (The cartoon in the inset shows the 3D coordinate system defining the orientations of the orthogonal views), (liver (L), intestine (I), spleen (S), aorta (A), tumour (T)) and quantifications of the MSOT signal intensity in aorta, different organs and tumour at different time points post-injection. Reprinted with permission from ref. [15]. Copyright 2015 WILEY-VCH Verlag GmbH & Co. KGaA, Weinheim. **f** Effect of PEG-modified gold nanotube pore size on myoglobin depth distribution inside the pores (mean ± SD, $n = 3$). Reprinted with permission from ref. [21]. Copyright 2012 Elsevier B.V

adamantine was chosen as the linker to assemble the porous Au/PtAu bimetallic heterojunction nanotube (PtAuBNTs) catalysts onto porcine reproductive and respiratory syndrome virus (PRRSV) antibody by Shao's group, which clearly surpassed the unstable electrostatic assembly between cationic surfactant and biosamples. The formed supramolecular "bridge" could extend the space to accommodate more PtAuBNTs catalysts and reduce the blocking effect. The fabricated sandwich immunosensor exhibited excellent analytical performance for PRRSV with a better linear detection range from 1:103 to 1:106 (dilution ratio) and a sensitive detection limit (10.8 pg/mL) [76]. However, there is not much research on gold nanotubes in this area. Aptasensors offer great potential to measure substances in clinical diagnostics, environmental analytics, food and biotechnology industries, process engineering and others. We look forward to the tremendous development of gold nanotube aptamer sensors in the future.

Photothermal therapy

Photothermal therapy (PPT) is a formidable candidate for cancer treatment because it can rely on laser-induced hyperthermia to kill cancer cells in the tumour area [96]. For clinical treatment, the penetration of near-infrared laser to human tissue is higher, and the damage is least [97]. Therefore, PPT as a minimally invasive treatment of cancer has been widely developed. Gold nanoparticles are particularly attractive for PPT because they have low cytotoxicity, biocompatibility and optical resonance wavelengths can be tuned over a broad range by controlling their sizes and shapes [97, 98], which open a treatment window for clinical oncology. For instance, Gold nanoparticles (~ 40 nm) convert light irradiation (514 nm) into heat energy that can kill cancer cells [99]. The SPR peak of gold nanotubes can be tuned in the range of 655 to 930 nm in the

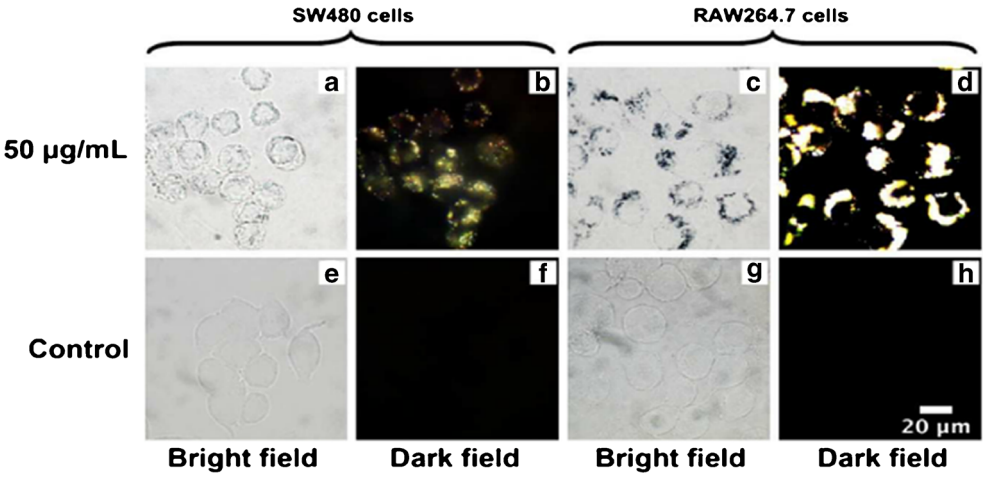

Fig. 12 Bright-field and dark-field microscopy images of SW480 and RAW 264.7 cells after incubation overnight in a medium containing Au NTs (~ 370 nm in length, Au mass fraction = 73.9%). All dark-field microscopy images are presented using the same brightness and contrast conditions. Reprinted with permission from ref. [16]. Copyright 2015 WILEY-VCH Verlag GmbH & Co. KGaA. Weinheim

near-infrared region, which offers potential advantages over their solid counterparts. Ye et al. [15] synthesized gold nanotube with controllable length, well-defined shape, high crystallinity and tunable near-infrared surface plasmon resonance. The AuNTs coated with poly (4-phenylene) improved the stability of the colloid and reduced the cytotoxicity. Cellular studies in vitro have shown that PSS-AuNTs not only uptake cancer cells (SW480 cells) and macrophages (RAW 264.7) (Fig. 11c, d), but also have biocompatibility (Fig. 12). Near-infrared laser irradiation can cause photothermal ablation of cancer cells internalizing PSS-AuNTs.

Imaging

Photoacoustic imaging (PAI) is a non-invasive and non-ionizing imaging method that combines the spectral selectivity of laser excitation with the high resolution of ultrasound imaging [100]. Considerable efforts have been made so far. For example, gold nanostructures such as gold nanorods, gold nanoshells, hollow gold nanospheres and gold nanocages have been developed. Gold nanotubes can exhibit exceptional surface-enhanced Raman scattering (SERS) and surface plasmon resonance (SPR) properties by modulating morphology**.** Near-infrared region can provide deeper radiation penetration through tissue and blood, which allowed the use of AuNTs for photothermal therapy and in vivo imaging with different techniques. Gold nanostructures in near-infrared absorbing have been developed to integrate targeting, imaging and therapy (chemotherapy through drug delivery and photothermal therapy) into one platform [101, 102]. The development of Au nanotubes as contrast agents is relied on the ability to tune their optical properties via control over the localized surface plasmon modes. Ye and co-workers synthesized gold nanotubes with controlled length and NIR absorption for the application as in vivo multispectral optoacoustic tomography (MSOT) contrast agents [15]. The gold nanotubes were subject to the surface modification of PSS coating, which offer colloidal stability and low cytotoxicity. In addition, PSS-AuNTs showed strong photoacoustic signal in vivo and accumulated in SW620 tumour, so it can be used as an effective photoacoustic imaging (PAI) contrast agent. In addition, the study on the biodistribution of PSS-AuNTs in vivo showed that PSS-AuNTs could clear the liver and gallbladder within 72 h, indicating that PSS-AuNTs was suitable for clinical transplantation. This work showed the effectiveness of gold nanotubes as a new reagent for photoacoustic imaging, in order to achieve image-guided chemical-photothermal combined therapy (Fig. 11e). As a promising contrast agent for biomedical and clinical applications, the hollow core of gold nanotube can reduce not only the heat capacity to allow better pulse heating but also the slender shape of gold nanotube that can improve the targeting efficiency. The PAI can also combine the therapeutic functions of AuNTs (such as photothermal therapy and drug delivery) to form a therapeutic nano platform for monitoring and treating diseases in a light controlled manner.

The rapid development of medical imaging technology has increased the accuracy and rapidity of disease diagnosis. Especially, optical imaging has made great progress. From X-ray to nuclear magnetic resonance, PET, E-PET, Raman imaging, fluorescence imaging, etc. Gold nanotubes can exhibit exceptional surface-enhanced Raman scattering (SERS) and surface plasmon resonance (SPR) properties by modulating morphology. Which means that gold nanotubes have strong potential in optical imaging. At present, the research on the combination of gold nanotube optical properties and imaging technology has a lot of space. In the future research, we look forward to the further development of gold nanotubes in Raman imaging and other fields.

Protein transport

Gold nanotubes are an ideal model system for protein transport because of unique tube structure. The gold nanotubes can act as a transport tool for ionic and molecular. Cai and coworkers studied adsorbate and defect effects on electronic and transport properties of gold nanotubes [103]. Ma et al. [21] demonstrated transport of single protein molecules inside gold nanotubes. They found that diffusion within PEG-coated gold nanotubes was two orders of magnitude faster than in previously reported and first demonstrated the influence of pore size on solo protein depth distribution. The result found that the number of protein molecules inside the pores were decreased with the depth increasing (Fig. 11f). Furthermore, protein transport can be finely controlled by gold nanotubes modified self-assembled monolayer.

Conclusion and outlook

In summary, we provide an update and in-depth review of some of the most exciting and important developments in the synthesis, properties and applications of gold nanotubes. We compared the two methods for the synthesis of gold nanotubes, which found that the hard template method is suitable for the synthesis of gold nanotubes array. The morphology of gold nanotubes arrays is fairly fixed, which have good dispersion and uniform pore diameter, but sources of template materials are relatively limited. The hard template method mainly be controlled by deposition time and gold plating solution. Nevertheless, the sacrificial template method is relatively flexible and easy to operate, which can achieve large-scale synthesis and be controlled by many factors, such as precursor template, the amount of chloroauric acid, reaction temperature, time and surfactant. At present, there are few systematic experimental studies on the precise control of the size, shape, wall thickness and the formation of pores of gold nanotubes by the sacrificial template method. The ultimate goal of producing gold nanotubes in a reliable, controllable and safe way is to develop a larger produced method, which is the basic requirement to promote the strong clinical application of gold nanotubes. Therefore, the preparation of gold nanotubes by the sacrificial template method deserves further study.

The SPR tunability and photophysical properties of gold nanoparticles make them an ideal candidate for many developments in a wide range of biological applications. Hollow gold nanoparticles prepared by using silver nanoparticles as templates have a variety of colours, such as light yellow, orange, burgundy, fuchsia, blue and even cyan. Xia's group demonstrated that the SPR peak shift of gold nanoshells exhibited higher sensitivity than solid gold nanoparticles with roughly the same sizes, which greatly improved sensitivity in optical response [104]. Based on this notation, AuNTs have great potentiality to be explored to optically detect binding events on their surfaces. Unfortunately, there are few applications of hollow AuNTs in biochemical detection. In the past, there has been a great surge in biosensor research base on AuNTs prepared by the hard template method. Much of these works have focused on electrochemical application. The surface area of the gold nanotube array electrode is much larger than that of the conventional electrode, which should be mainly responsible for the high sensitivity. However, optical sensors offer a combination of fast response, high sensitivity and immunity to electromagnetic interference and provide additional options for signal retrieval, such as optical intensity, spectrum and polarization compared with electrochemical sensors [105]. Plasmonics has been attracting increasing attention for the development of optical sensors due to the ability to confine and enhance electromagnetic fields. The biomedical application of optical sensor made with gold nanotube is just the tip of the iceberg.

The applications of photothermal properties of gold solid nanoparticles, hollow gold nanoshells and gold nanocages in nanomedicine were compared with experiments and computer simulation [106]. Researchers found that gold nanocages produced the highest temperature under 808 nm CW laser irradiation. For hollow, non-porous or microporous gold nanoshells, there is a certain range of wall thickness. Computer simulation predicted that increasing the porosity of the nanoshells wall leads to the overall improvement of its photothermal efficiency. In the hollow gold nanostructures synthesized by galvanic replacement reaction, the residual silver is the possible reason that limits the movement of SPR to the near-infrared spectrum region. Therefore, it is necessary to gradually simulate the optical properties of gold nanostructures during the preparation process, and optimize the corresponding production process of Gold nanotubes. This is very important for the application of nanomedicine. In addition, surface functional modification is another key point. Biocompatibility of gold nanotubes, the ability to uptake cancer cells and macrophages, the ability to transport proteins, and the ability to deliver drugs depend on their functional types.

As indicated above, on the one hand, looking for cheap, nontoxic and stable template is the research hotspot of template method. It is of practical value to further study the reaction mechanism of templates by selecting appropriate soft or hard templates and changing reaction conditions. On the other hand, the gold nanotubes provide not only larger active areas and more electroactive sites for immobilizing biomolecules, but also good biocompatibility. At present, the applications of gold nanotube mainly focus on catalysis, contrast agents, photothermal therapy and electrochemical sensing. However, there are few studies using them as surface plasmon resonance (SPR), fluorescence and surface-enhanced Raman scattering (SERS) probes. As researchers continue to explore

this promising material, we believe the unique features of AuNTs and numerous ways in which the properties can be tuned will likely lead to the development of further exciting techniques and powerful combinations of existing ones.

Compliance with ethical standards

Conflict of interest The authors declare that they have no competing of interests.

References

1. Iijima S (1991) Helical microtubes of graphite carbon. Nature 354(6348):56–58
2. Dreaden EC, Alkilany AM, Huang X, Murphy CJ, El-Sayed MA (2012) The golden age: gold nanoparticles for biomedicine. Chem Soc Rev 41(7):2740–2779
3. Luo P, Liu Y, Xia Y, Xu H, Xie G (2014) Aptamer biosensor for sensitive detection of toxin a of Clostridium difficile using gold nanoparticles synthesized by Bacillus stearothermophilus. Biosens Bioelectron 54:217–221
4. Wang Y, Black KCL, Luehmann H, Li W, Zhang Y, Cai X, Wan D, Liu S-Y, Li M, Kim P, Li Z-Y, Wang LV, Liu Y, Xia Y (2013) Comparison study of gold Nanohexapods, Nanorods, and Nanocages for Photothermal Cancer treatment. ACS Nano 7(3): 2068–2077
5. Huang L, Zou J, Ye JY, Zhou ZY, Lin Z, Kang X, Jain PK, Chen S (2019) Synergy between Plasmonic and Electrocatalytic activation of methanol oxidation on palladium–silver alloy nanotubes. Angew Chem Int Ed 58(26):8794–8798
6. Liu J, Detrembleur C, De Pauw-Gillet MC, Mornet S, Jerome C, Duguet E (2015) Gold nanorods coated with mesoporous silica shell as drug delivery system for remote near infrared light-activated release and potential phototherapy. Small 11(19): 2323–2332
7. Wang JZG, You M (2012) Assembly of Aptamer switch probes and photosensitizer on gold Nanorods for targeted photothermal and photodynamic cancer therapy. ACS Nano 6(6):5070–5077
8. Zierold R, Nielsch K (2011) Tailor-made, magnetic nanotubes by template-directed atomic layer deposition. ECS Trans 41(2):111–121
9. Bi Y, Lu G (2008) Controlled synthesis of pentagonal gold nanotubes at room temperature. Nanotechnology 19(27):275306
10. Kohli P, Wharton JE, Braide O, Martin CR (2004) Template synthesis of gold nanotubes in an anodic alumina membrane. J Nanosci Nanotechnol 4(6):605–610
11. Chen J, Wiley BJ, Xia Y (2007) One-dimensional nanostructures of metals: large-scale synthesis and some potential applications. Langmuir 23(8):4120–4129
12. Sun Y, Mayers BT, Xia Y (2002) Template-engaged replacement reaction: a one-step approach to the large-scale synthesis of metal nanostructures with hollow interiors. Nano Lett 2(5):481–485
13. Through N (2002) Large-scale synthesis of uniform silver. Adv Mater 11:833–837
14. Zhu J (2009) Composition-dependent plasmon shift in Au-Ag alloy nanotubes: effect of local field distribution. J Phys Chem C 113(8):3164–3167
15. Ye S, Marston G, McLaughlan JR, Sigle DO, Ingram N, Freear S, Baumberg JJ, Bushby RJ, Markham AF, Critchley K, Coletta PL, Evans SD (2015) Engineering gold nanotubes with controlled length and near-infrared absorption for theranostic applications. Adv Funct Mater 25(14):2117–2127
16. Mashentseva A, Borgekov D, Kislitsin S, Zdorovets M, Migunova A (2015) Comparative catalytic activity of PET track-etched membranes with embedded silver and gold nanotubes. Nucl Instrum Methods Phys Res, Sect B 365:70–74
17. Wirtz M, Parker M, Kobayashi Y, Martin CR (2002) Template-synthesized nanotubes for chemical separations and analysis. Chem Eur J 8(16):3572–3578
18. Chen A, Ding Y, Yang Z, Yang S (2015) Constructing heterostructure on highly roughened caterpillar-like gold nanotubes with cuprous oxide grains for ultrasensitive and stable non-enzymatic glucose sensor. Biosens Bioelectron 74:967–973
19. Costa JCS, Corio P, Rossi LM (2015) Catalytic oxidation of cinnamyl alcohol using Au-Ag nanotubes investigated by surface-enhanced Raman spectroscopy. Nanoscale 7(18):8536–8543
20. Ye S, Marston G, Markham AF, Louise Coletta P, Evans SD (2019) Developing gold nanotubes as photoacoustic contrast agents. J Phys Conf Ser 1151:012018
21. Ma C, Han R, Qi S, Yeung ES (2012) Selective transport of single protein molecules inside gold nanotubes. J Chromatogr A 1238: 11–14
22. Li HH, Yu SH (2019) Recent advances on controlled synthesis and engineering of hollow alloyed nanotubes for Electrocatalysis. Adv Mater 31(38):e1803503
23. Dong W, Dong H, Wang Z, Zhan P, Yu Z, Zhao X, Zhu Y, Ming N (2006) Ordered array of gold nanoshells interconnected with gold nanotubes fabricated by double templating. Adv Mater 18(6):755–759
24. Walker SA, Zasadzinski JA, Glinka C, Nicol J, Margolese D, Stucky GD, Chmelka BF (1995) Cooperative Organization of Inorganic-Surfactant and Biomimetic Assemblies. Science 267(5201):1138–1143
25. Qian XF, Yin J, Feng S, Liu SH, Zhu ZK (2001) Preparation and characterization of polyvinylpyrrolidone films containing silver sulfide nanoparticles. J Mater Chem 11(10):2504–2506
26. AlMawlawi D, Coombs N, Moskovits M (1991) Magnetic properties of Fe deposited into anodic aluminum oxide pores as a function of particle size. J Appl Phys 70(8):4421–4425
27. Zhang X, Wang H, Bourgeois L, Pan R, Zhao D, Webley PA (2008) Direct electrodeposition of gold nanotube arrays for sensing applications. J Mater Chem 18(4):463–467
28. Bridges CR, DiCarmine PM, Seferos DS (2012) Gold nanotubes as sensitive, solution-Suspendable refractive index reporters. Chem Mater 24(6):963–965
29. Al-Kaysi RO, Ghaddar TH, Guirado G (2009) Fabrication of one-dimensional organic nanostructures using anodic aluminum oxide templates. J Nanomater 2009:7
30. McPhillips J, Murphy A, Jonsson MP, Hendren WR, Atkinson R, Höök F, Zayats AV, Pollard RJ (2010) High-performance biosensing using arrays of plasmonic nanotubes. ACS Nano 4(4): 2210–2216
31. Murphy A, McPhillips J, Hendren W, McClatchey C, Atkinson R, Wurtz G, Zayats AV, Pollard RJ (2011) The controlled fabrication and geometry tunable optics of gold nanotube arrays. Nanotechnology 22(4):045705
32. Hendren WR, Murphy A, Evans P, O'Connor D, Wurtz GA, Zayats AV, Atkinson R, Pollard RJ (2008) Fabrication and optical properties of gold nanotube arrays. J Phys Condens Matter 20(36): 362203
33. Tian T, Dong J, Xu J (2016) Direct electrodeposition of highly ordered gold nanotube arrays for use in non-enzymatic amperometric sensing of glucose. Microchim Acta 183(6):1925–1932
34. Yang G, Yang X, Yang C, Yang Y (2011) A reagentless amperometric immunosensor for human chorionic gonadotrophin based on a gold nanotube arrays electrode. Colloids Surf A Physicochem Eng Asp 389(1–3):195–200

35. Yang G, Chen Y, Li L, Yang Y (2011) Direct electrochemical determination of morphine on a novel gold nanotube arrays electrode. Clin Chim Acta 412(17–18):1544–1549
36. Yang G, Li L, Jiang J, Yang Y (2012) Direct electrodeposition of gold nanotube arrays of rough and porous wall by cyclic voltammetry and its applications of simultaneous determination of ascorbic acid and uric acid. Mater Sci Eng C 32(6):1323–1330
37. Shariati M, Ghorbani M, Sasanpour P, Karimizefreh A (2019) An ultrasensitive label free human papilloma virus DNA biosensor using gold nanotubes based on nanoporous polycarbonate in electrical alignment. Anal Chim Acta 1048:31–41
38. Bridges CR, DiCarmine PM, Fokina A, Huesmann D, Seferos DS (2013) Synthesis of gold nanotubes with variable wall thicknesses. J Mater Chem A 1(4):1127–1133
39. Fleischer RL, Buford Price P, Walker RW (1975) Nuclear tracks in solids: principles and applications. University of California Press, Berkeley 40 (6):697
40. Fink D, Chandra A, Alegaonkar P, Berdinsky A, Petrov A, Sinha D (2007) Nanoclusters and nanotubes for swift ion track technology. Radiat Eff Defects Solids 162(3–4):151–156
41. Mashentseva AA, Korolkov IV, Yeszhanov AB, Zdorovets MV, Russakova AV (2019) The application of composite ion track membranes with embedded gold nanotubes in the reaction of aminomethylation of acetophenone. Mater Res Express 6(11): 115022
42. Bahari Mollamahalle Y, Ghorbani M, Dolati A (2012) Electrodeposition of long gold nanotubes in polycarbonate templates as highly sensitive 3D nanoelectrode ensembles. Electrochim Acta 75:157–163
43. Wang HW, Shieh CF, Chen HY, Shiu WC, Russo B, Cao G (2006) Standing [111] gold nanotube to nanorod arrays via template growth. Nanotechnology 17(10):2689–2694
44. Barreca D, Gasparotto A, Maragno C, Tondello E (2005) Synthesis of gold nanotubes by sputtering of gold into porous materials. J Nanosci Nanotechnol 5(11):1883–1886
45. Mollamahale YB, Ghorbani M, Ghalkhani M, Vossoughi M, Dolati A (2013) Highly sensitive 3D gold nanotube ensembles: application to electrochemical determination of metronidazole. Electrochim Acta 106:288–292
46. Baker LA, Jin P, Martin CR (2005) Biomaterials and biotechnologies based on nanotube membranes. Crit Rev Solid State Mater Sci 30(4):183–205
47. Pyo M, Joo J, Youn SJ (2007) Simultaneous control of Au nanotube lengths and pore sizes with a single kind of polycarbonate membrane via interfacial deposition at the air/water interface. Bull Kor Chem Soc 28(8):1285–1288
48. Tao M, Li X, Wu Z, Wang M, Hua M, Yang Y (2011) The preparation of label-free electrochemical immunosensor based on the Pt-Au alloy nanotube array for detection of human chorionic gonadotrophin. Clin Chim Acta 412(7–8):550–555
49. Siwy Z, Trofin L, Kohli P, Baker LA, Trautmann C, Martin CR (2005) Protein biosensors 'based on biofunctionalized conical gold nanotubes. J Am Chem Soc 127(14):5000–5001
50. Sun Y, Xia Y (2004) Multiple-walled nanotubes made of metals. Adv Mater 16(3):264–268
51. Luo M, Zhou M, Da Silva RR, Tao J, Figueroa-Cosme L, Gilroy KD, Peng HC, He Z, Xia Y (2017) Pentatwinned cu nanowires with ultrathin diameters below 20 nm and their use as templates for the synthesis of au-based nanotubes. ChemNanoMat 3(3):190–195
52. Kim HW, Lee JW, Kebede MA, Kim HS, Srinivasa B, Kong MH, Lee C (2008) Fabrication of gold nanotubes from removable MgO nanowires templates. J Nanosci Nanotechnol 8(11):5715–5719
53. Ballabh R, Nara S (2015) Template based synthesis of gold nanotubes using biologically synthesized gold nanoparticles. Indian J Exp Biol 53(12):828–833
54. Lu MY, Chang YC, Chen LJ (2006) Synthesis of Au nanotubes with SiOx nanowires as sacrificial templates. J Vac Sci Technol A 24(4):1336–1339
55. Schwartzberg AM, Olson TY, Talley CE, Zhang JZ (2007) Gold nanotubes synthesized via magnetic alignment of cobalt nanoparticles as templates. J Phys Chem C 111(44):16080–16082
56. Hunyadi SE, Murphy CJ (2006) Bimetallic silver-gold nanowires: fabrication and use in surface-enhanced Raman scattering. J Mater Chem 16(40):3929–3935
57. Zhu H, Chen H, Wang J, Li Q (2013) Fabrication of Au nanotube arrays and their plasmonic properties. Nanoscale 5(9):3742–3746
58. Sun XM, Li YD (2005) Cylindrical silver nanowires: preparation, structure, and optical properties. Adv Mater 17(21):2626–2630
59. El Mel AA, Chettab M, Gautron E, Chauvin A, Humbert B, Mevellec JY, Delacote C, Thiry D, Stephant N, Ding J, Du K, Choi CH, Tessier PY (2016) Galvanic replacement reaction: a route to highly ordered bimetallic nanotubes. J Phys Chem C 120(31):17652–17659
60. Sun Y (2010) Silver nanowires - unique templates for functional nanostructures. Nanoscale 2(9):1626–1642
61. Gu X, Cong X, Ding Y (2010) Platinum-decorated Au porous nanotubes as highly efficient catalysts for formic acid electro-oxidation. ChemPhysChem 11(4):841–846
62. Sun H, Guo X, Ye W, Kou S, Yang J (2016) Charge transfer accelerates galvanic replacement for PtAgAu nanotubes with enhanced catalytic activity. Nano Res 9(4):1173–1181
63. Guan S, Fu X, Tang Y, Peng Z (2017) AuAg@CdS double-walled nanotubes: synthesis and nonlinear absorption properties. Nanoscale 9(29):10277–10284
64. Guan S, Fu X, Tang Y, Peng Z (2017) Synthesis and photoeletrochemical performance of AuAg@CdS double-walled nanotubes. Chem Phys Lett 682:128–132
65. Kundu S, Patra A (2017) Nanoscale strategies for light harvesting. Chem Rev 117(2):712–757
66. Wiley B, Herricks T, Sun Y, Xia Y Polyol synthesis of silver nanoparticles: use of chloride and oxygen to promote the formation of single-crystal, truncated cubes and tetrahedrons. Nano Lett 4(10):2057–2057
67. Rodrigues TS, Silva AGM, Moura ABL, Geonmonond RS, Camargo PHC (2016) AgAu nanotubes: investigating the effect of surface morphologies and optical properties over applications in catalysis and photocatalysis. J Braz Chem Soc 28(9):1630–1638
68. Sun Y, Xia Y (2004) Mechanistic study on the replacement reaction between silver nanostructures and chloroauric acid in aqueous medium. J Am Chem Soc 126(12):3892–3901
69. Skrabalak SE, Au L, Li X, Xia Y (2007) Facile synthesis of Ag nanocubes and Au nanocages. Nat Protoc 2(9):2182–2190
70. Gu X, Xu L, Tian F, Ding Y (2009) Au-Ag alloy nanoporous nanotubes. Nano Res 2(5):386–393
71. Sun Y, Mayers B, Xia Y (2003) Metal nanostructures with hollow interiors. Adv Mater 15(78):641–646
72. Margalit S, Avraham S, Shahal T, Michaeli Y, Gilat N, Magod P, Caspi M, Loewenstein S, Lahat G, Friedmann-Morvinski D, Kariv R, Rosin-Arbesfeld R, Zirkin S, Ebenstein Y (2019) 5-Hydroxymethylcytosine as a clinical biomarker: fluorescence-based assay for high-throughput epigenetic quantification in human tissues. Int J Cancer 146(1):115–122
73. Yang A, Bi J, Yang S, Zhang J, Chen A, Liang S (2014) Highly surface-roughened caterpillar-like Au/Ag nanotubes for sensitive and reproducible substrates for surface enhanced Raman spectroscopy. RSC Adv 4(86):45856–45861
74. Yin X, Teradal NL, Jelinek R (2017) Porous gold nanotubes for enhanced methanol oxidation catalysis. ChemistrySelect 2(34): 10961–10964

75. Zhou Z, Zhang F, Wang J, Zhang X, Xu W, Wu R, Liao L, Wang X, Wei J (2019) L-cysteine modified ZnO: small change while great progress. Mater Sci Eng C Mater Biol Appl 103:109818
76. Shao K, Zhang C, Ye S, Cai K, Wu L, Wang B, Zou C, Lu Z, Han H (2017) Near–infrared electrochemiluminesence biosensor for high sensitive detection of porcine reproductive and respiratory syndrome virus based on cyclodextrin-grafted porous Au/PtAu nanotube. Sensors Actuators B Chem 240:586–594
77. Ocwieja M, Barbasz A, Walas S, Roman M, Paluszkiewicz C (2017) Physicochemical properties and cytotoxicity of cysteine-functionalized silver nanoparticles. Colloids Surf B Biointerfaces 160:429–437
78. Liu H, Li Z, Yan Y, Zhao J, Wang Y (2019) Chiroptical study of bimetal-cysteine hybrid composite: interaction between cysteine and Au/Ag alloyed nanotubes. Nanoscale 11(45):21990–21998
79. Zhu J (2007) Theoretical study of the light scattering from gold nanotubes: effects of wall thickness. Mater Sci Eng 454:685–689
80. Zhao S, Zhu J (2017) The effect of local dielectric environment on the resonance light scattering of Au–Ag bimetallic nanotube. Appl Phys A 123(12):1–9
81. Velichko EA (2014) Plasmon resonances in the scattering and absorption of light by a circular gold nanotube. 2014 IEEE 34th International Scientific Conference on Electronics and Nanotechnology, ELNANO 2014 - Conference Proceedings:42–45
82. Xu H, Li H, Liu Z, Xie S, Zhou X, Wu J (2011) Adjustable plasmon resonance in the coaxial gold nanotubes. Solid State Commun 151(10):759–762
83. Costa JCS, Corio P, Camargo PHC (2012) Silver-gold nanotubes containing hot spots on their surface: facile synthesis and surface-enhanced Raman scattering investigations. RSC Adv 2(26):9801–9804
84. Choi Y, Baker LA, Hillebrenner H, Martin CR (2006) Biosensing with conically shaped nanopores and nanotubes. Phys Chem Chem Phys 8(43):4976–4988
85. Zhai J, Cui H, Yang R (1997) DNA based biosensors. Biotechnol Adv 15(1):43–58
86. McCooey A (2015) High sensitivity nucleic acid detection using metal nanowires and nanotubes. phD thesis, Dublin city university
87. WHO global tuberculosis report (2014) https://www.who.int/tb/publications/global_report/archive/en/
88. Torati SR, Reddy V, Yoon SS, Kim C (2016) Electrochemical biosensor for mycobacterium tuberculosis DNA detection based on gold nanotubes array electrode platform. Biosens Bioelectron 78:483–488
89. Li X, Cao L, Zhang Y, Yan P, Kirk DW (2017) Fabrication and modeling of an ultrasensitive label free impedimetric immunosensor for Aflatoxin B1 based on protein a self-assembly modified gold 3D nanotube electrode ensembles. Electrochim Acta 247:1052–1059
90. Bhakta SA, Evans E, Benavidez TE, Garcia CD (2015) Protein adsorption onto nanomaterials for the development of biosensors and analytical devices: a review. Anal Chim Acta 872:7–25
91. Sexton LT, Horne LP, Sherrill SA, Bishop GW, Baker LA, Martin CR (2007) Resistive-pulse studies of proteins and protein/antibody complexes using a conical nanotube sensor. J Am Chem Soc 129(43):13144–13152
92. Movileanu L, Howorka S, Braha O, Bayley H (2000) Detecting protein analytes that modulate transmembrane movement of a polymer chain within a single protein pore. Nat Biotechnol 18(10):1091–1095
93. Björck L, Kronvall GP (1984) Purification and some properties of streptococcal protein G, a novel IgG-binding reagent. J Immunol 133(2):969–974
94. Poli MA, Victor RR, John FH, Gerald AM Detection of ricin by colorimetric and chemiluminescence ELISA. Toxicon Off J Int Soc Toxinol 32(11):0–1377
95. Hong P, Li W, Li J (2012) Applications of aptasensors in clinical diagnostics. Sensors 12(2):1181–1193
96. Tang P, Liu Y, Liu Y, Meng H, Liu Z, Li K, Wu D (2019) Thermochromism-induced temperature self-regulation and alternating photothermal nanohelix clusters for synergistic tumor chemo/photothermal therapy. Biomaterials 188:12–23
97. Jabeen F, Najam-ul-Haq M, Javeed R, Huck CW, Bonn GK (2014) Au-nanomaterials as a superior choice for near-infrared photothermal therapy. Molecules 19(12):20580–20593
98. Hu Y, Liu X, Cai Z, Zhang H, Gao H, He W, Wu P, Cai C, Zhu J-J, Yan Z (2018) Enhancing the plasmon resonance absorption of multibranched gold nanoparticles in the near-infrared region for photothermal cancer therapy: theoretical predictions and experimental verification. Chem Mater 31(2):471–482
99. Hainfeld JF, Lin L, Slatkin DN, Avraham Dilmanian F, Vadas TM, Smilowitz HM (2014) Gold nanoparticle hyperthermia reduces radiotherapy dose. Nanomedicine 10(8):1609–1617
100. Maji SK, Sreejith S, Joseph J, Lin M, He T, Tong Y, Sun H, Yu SW-K, Zhao Y (2014) Upconversion nanoparticles as a contrast agent for photoacoustic imaging in live mice. Adv Mater 26(32):5633–5638
101. Huang X, Neretina S, El-Sayed MA (2010) Gold nanorods: from synthesis and properties to biological and biomedical applications. Adv Mater 21(48):4880–4910
102. Bardhan R, Lal S, Joshi A, Halas NJ (2011) Theranostic Nanoshells: from probe design to imaging and treatment of Cancer. Acc Chem Res 44(10):936–946
103. Cai Y, Zhou M, Zeng M, Zhang C, Feng YP (2011) Adsorbate and defect effects on electronic and transport properties of gold nanotubes. Nanotechnology 22(21):215702
104. Sun Y, Xia Y (2011) Synthesis of gold nanoshells and their use in sensing applications MRS proceedings 776
105. Wang P, Nasir ME, Krasavin AV, Dickson W, Jiang Y, Zayats AV (2019) Plasmonic metamaterials for nanochemistry and sensing. Acc Chem Res 52:3018–3028
106. Lopatynskyi AM, Malymon YO, Lytvyn VK, Mogylnyi IV, Rachkov AE, Soldatkin AP, Chegel VI (2017) Solid and hollow gold nanostructures for Nanomedicine: comparison of photothermal properties. Plasmonics 13(5):1659–1669